

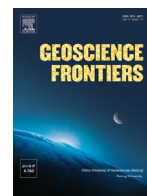
HOSTED BY



ELSEVIER

Contents lists available at ScienceDirect

Geoscience Frontiers

journal homepage: www.elsevier.com/locate/gsf

Geologic field evidence for non-lithostatic overpressure recorded in the North American Cordillera hinterland, northeast Nevada

Andrew V. Zuza^{a,*}, Drew A. Levy^a, Suzanne R. Mulligan^b

^a Nevada Bureau of Mines and Geology, University of Nevada, Reno, NV 89557, USA

^b Department of Geoscience, University of Nevada, Las Vegas, NV 89154, USA

ARTICLE INFO

Article history:

Received 25 March 2020

Received in revised form 16 September 2020

Accepted 17 October 2020

Available online xxxx

Handling Editor: M. Santosh

Keywords:

Non-lithostatic pressure

Tectonic overpressure

North American Cordillera

Ruby Mountain-East Humboldt Range

Peak temperature

Geothermal gradient

ABSTRACT

There is a long-standing discrepancy for numerous North American Cordillera metamorphic core complexes between geobarometric pressures recorded in the exhumed rocks and their apparent burial depths based on palinspastic reconstructions from geologic field data. In particular, metamorphic core complexes in eastern Nevada are comprised of well-documented ~12–15 km thick Neoproterozoic–Paleozoic stratigraphy of Laurentia's western passive margin, which allows for critical characterization of field relationships. In this contribution we focus on the Ruby Mountain–East Humboldt Range–Wood Hills–Pequop Mountains (REWP) metamorphic core complex of northeast Nevada to explore reported peak pressure estimates versus geologic field relationships that appear to prohibit deep burial. Relatively high pressure estimates of 6–8 kbar (23–30 km depth, if lithostatic) from the lower section of the Neoproterozoic–Paleozoic passive margin sequence require burial and or repetition of the passive margin sequence by 2–3× stratigraphic depths. Our observations from the least migmatized and/or mylonitized parts of this complex, including field observations, a transect of peak-temperature (T_p) estimates, and critical evaluation of proposed thickening/burial mechanisms cannot account for such deep burial. From Neoproterozoic–Cambrian (c) rocks part of a continuous stratigraphic section that transitions ~8 km upsection to unmetamorphosed Permian strata that were not buried, we obtained new quartz-in-garnet barometry via Raman analysis that suggest pressures of ~7 kbar (~26 km). A T_p traverse starting at the same basal c rocks reveals a smooth but hot geothermal gradient of ~40 °C/km that is inconsistent with deep burial. This observation is clearly at odds with thermal gradients implied by high P - T estimates that are all ≤25 °C/km. Remarkably similar discrepancies between pressure estimates and field observations have been discussed for the northern Snake Range metamorphic core complex, ~200 km to the southeast. We argue that a possible reconciliation of long-established field observations versus pressures estimated from a variety of barometry techniques is that the rocks experienced non-lithostatic tectonic overpressure. We illustrate how proposed mechanisms to structurally bury the rocks, as have been invoked to justify published high pressure estimates, are entirely atypical of the Cordillera hinterland and unlike structures interpreted from other analogous orogenic plateau hinterlands. Proposed overpressure mechanisms are relevant in the REWP, including impacts from deviatoric/differential stress considerations, tectonic mode switching, and the autoclave effect driven by dehydration melting. Simple mechanical arguments demonstrate how this overpressure could have been achieved. This study highlights that detailed field and structural restorations of the least strained rocks in an orogen are critical to evaluate the tectonic history of more deformed rocks.

© 2021 China University of Geosciences (Beijing) and Peking University. Production and hosting by Elsevier B.V. This is an open access article under the CC BY-NC-ND license (<http://creativecommons.org/licenses/by-nc-nd/4.0/>).

1. Introduction

Whether pressure recorded by metamorphic rocks represents lithostatic pressures, and thus depth, is debated (e.g., Petrini and Podladchikov, 2000; Moulas et al., 2013; Schmalholz and Podladchikov, 2013; Gerya, 2015). Non-lithostatic pressure describes when total pressure expressed in the rock record (sometimes referred to as dynamic pressure, e.g., Marques et al., 2018) deviates from

lithostatic pressures, and this difference is commonly referred to as tectonic under- or overpressure. Herein, we use the term non-lithostatic pressure instead of tectonic underpressure or overpressure to focus more broadly than just tectonic-caused differences between lithostatic and total pressure. The occurrence of non-lithostatic pressure has been investigated primarily by analytical and numerical models (see Schmalholz and Podladchikov, 2013; Gerya, 2015), which suggest the potential for a twofold difference between lithostatic and mean stress (pressure). Studies that attempt to estimate the relationship between pressure and depth with field documentation and evidence are relatively few, including in the Alps (Pleuger and Podladchikov, 2014;

* Corresponding author.

E-mail address: azuza@unr.edu (A.V. Zuza).

<https://doi.org/10.1016/j.gsf.2020.10.006>

1674-9871/© 2021 China University of Geosciences (Beijing) and Peking University. Production and hosting by Elsevier B.V. This is an open access article under the CC BY-NC-ND license (<http://creativecommons.org/licenses/by-nc-nd/4.0/>).

Luisier et al., 2019), Himalaya (Marques et al., 2018), and for Appalachian eclogites (Chu et al., 2017). These examples are focused on continental subduction systems with very deep proposed burial, and whether non-lithostatic pressures similarly occur in Cordillera-type retroarc fold-thrust systems is entirely unexplored. Regardless of tectonic setting, more examples and field-based confirmation of non-lithostatic pressure in the metamorphic rock record are necessary to support and validate its existence in nature. If significant overpressure occurs in the geologic record, even if infrequently, there are profound implications for reconstruction of tectonic burial and exhumation in mountain belts and subduction zones.

In the hinterland of the North American Cordillera, eastern Nevada, the well characterized 12–15-km thick Neoproterozoic–Triassic passive margin sequence (Stewart and Poole, 1974) represents a useful structural marker for palinspastic reconstructions of Mesozoic contractional deformation and crustal thickening, and subsequent Cenozoic extension (e.g., Armstrong and Hansen, 1966; Coney and Harms, 1984; Miller and

Gans, 1989). Geobarometric data from the Ruby Mountains–East Humboldt Range–Wood Hills–Pequop Mountains (REWP) and Snake Range metamorphic core complexes of eastern Nevada suggest that this passive margin sequence was buried to great depths (>30 km) by the Late Cretaceous and later exhumed to the surface via high-magnitude Cenozoic extension (Hodges et al., 1992; Lewis et al., 1999; Cooper et al., 2010; McGrew et al., 2000) (Fig. 1). These pressure estimates have long been at odds with field-based reconstructions that suggest these rocks were never buried much deeper than original stratigraphic depths (e.g., Miller and Gans, 1989; Thorman et al., 1990; Colgan et al., 2010) (e.g., Fig. 1C and D). These discrepancies have been reconciled with cryptic overthrust panels that have since been extended and/or eroded away to remove any trace of their existence (Camilleri and Chamberlain, 1997; Lewis et al., 1999). However, regional compilations of erosion levels beneath Cenozoic rocks suggest no trace of these inferred major structures (Armstrong, 1968; Gans and Miller, 1983; Van Buer et al., 2009; Long, 2012).

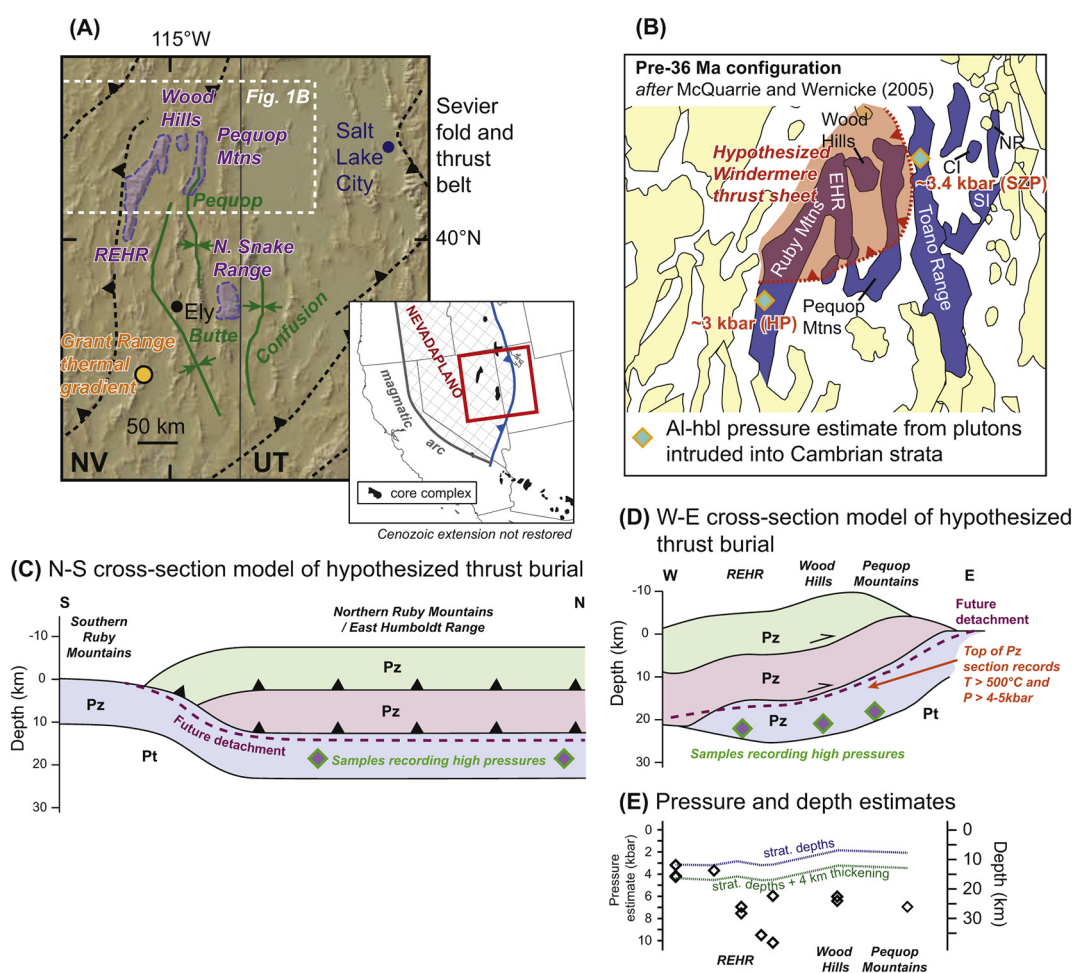


Fig. 1. (A) Metamorphic core complexes in northeastern Nevada in the hinterland of the Sevier fold-thrust belt, including the Ruby Mountains–East Humboldt Range–Pequop Mountains (REWP) and northern Snake Range. Approximate location of Fig. 1B shown with white box. Orange symbol shows Grant Range study area of Long and Soignard (2016), which derived a geothermal gradient of 50–60 °C/km as discussed in the text and Fig. 3C. Inset shows location of Fig. 1A in context of western North America. (B) Pre-extensional restoration of McQuarrie and Wernicke (2005) showing approximate distribution of ranges in northern Nevada; modified slightly to show less extension because well data does not support complete closure of the basins. Red polygon shows hypothesized trace of the Windermere thrust sheet to bury the local stratigraphy to great depths. Ranges in blue experienced Jurassic deformation associated with Elko orogeny. Note that some ranges in northeast Nevada were probably overlapping prior to Cenozoic extension, and thus exposures across each range may correlate vertically or laterally. Aluminum-in-hornblende pressure estimates from plutons that intruded into Cambrian strata, shown with green-orange diamonds, suggest that the Paleozoic stratigraphy was buried slightly deeper (several km) than stratigraphic depths. HP–Eocene Harrison Pass pluton; SZP–Late Jurassic Silver Zone Pass pluton; SI–Silver Island Range; CI–Crater Island Mountains; NR–Newfoundland Range. (C) Sketch of thrust-burial model along a north-south cross section to explain high pressures recorded in samples from the REWP, requiring 2–3× duplication of the Paleozoic stratigraphic. The southern Ruby Mountains were not buried (e.g., Colgan et al., 2010), which requires a sharp gradient from deep burial to minimal burial. (D) Sketch of thrust-burial model along a west-east cross section to explain REWP high pressures. The cross section was drafted at the same spatial extent as the plot in Fig. 1E. (E) Approximate location of peak-pressure samples along a west-east transect. Blue line shows expected pressure and depths for each sample based on its stratigraphic position, and the green line shows the expected pressure and depths based on stratigraphic position and +4 km thrust burial. Data in Table 1 and discussed in the text. (For interpretation of the references to color in this figure legend, the reader is referred to the web version of this article.)

In this contribution, we synthesize existing pressure estimates from the REWP metamorphic core complex, which span ~6–8+ kbar with a few lower pressure (3–4 kbar) exceptions (Fig. 1E), conduct new Raman quartz inclusion and aluminum-in-hornblende barometry to supplement published datasets, and use field-based evidence from our recent 1:24,000-scale mapping of the region (Henry and Thorman, 2015; Zuza et al., 2018, 2019a, 2020; Fig. 2) to suggest that much of

the passive margin stratigraphy was never buried significantly deeper than original stratigraphic depths. Accordingly, we argue that one explanation to reconcile field observations with published pressures estimated from a variety of barometry techniques is that the rocks experienced non-lithostatic overpressure, such that the recorded total pressures are greater than lithostatic pressure, thus providing a field example of this phenomenon. Our interpretation is further supported by

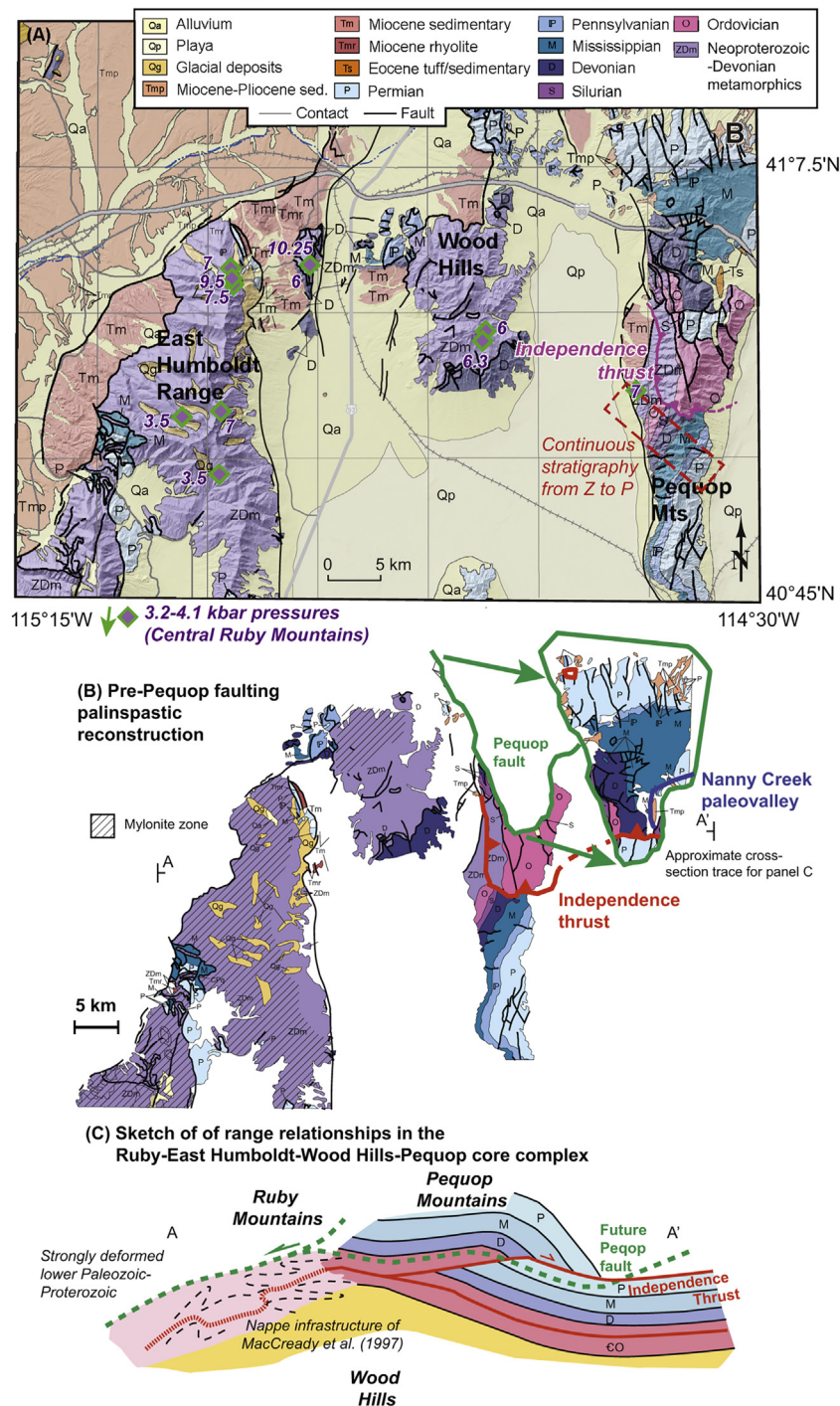


Fig. 2. (A) Geologic map of northeastern Nevada, simplified from Crafford (2007), showing the Ruby Mountains, East Humboldt Range, Wood Hills, and northern Pequop Mountains. Our new 1:24,000-scale mapping covers much of the Pequop Mountains (Henry and Thorman, 2015; Dee et al., 2017; Zuza et al., 2018, 2019a). (B) Palinspastic reconstruction of the REWP metamorphic core complex, including the juxtaposition of constituent ranges, restoration of the Pequop normal fault, and alignment of the Independence thrust observed in the Pequop Mountains and the hanging wall of the Pequop fault. Line A-A' is the cross-section line for Fig. 2C. (C) Cross-section model based on the geology in Fig. 2B, demonstrating how the Independence thrust (red) roots into the strongly deformed nappe structures of the Ruby Mountains-East Humboldt Range and the geometry of the Cenozoic normal fault systems (dashed green) with a breakaway east of the Pequop Mountains. We infer the nappe structures of MacCready et al. (1997) in the Ruby Mountains, although this aspect remains speculative.

new thermochronology from across the region, and a peak temperature traverse across the Neoproterozoic–Paleozoic strata that refutes its burial to 2× or 3× original stratigraphic depth. This example suggests that, whenever possible, tectonic reconstructions incorporating geobarometric estimates should adhere to established field relationships and structural observations.

2. Published models for non-lithostatic pressure

Non-lithostatic pressure, commonly discussed as tectonic overpressure, remains a controversial topic, but there is a growing body of literature over the past ~15 years describing possible mechanisms. End-member categories for non-lithostatic pressure are based on thermodynamics, mechanical arguments, or tectonic/structural setting. Here we briefly summarize these main non-lithostatic pressure arguments, which can be grouped into roughly five categories: (1) non-hydrostatic thermodynamics (e.g., Wheeler, 2014); (2) deviatoric stress considerations (Pettrini and Podladchikov, 2000); (3) significant rock strength or viscosity contrasts (e.g., Schmid and Podladchikov, 2003; Luisier et al., 2019); (4) tectonic mode switching (Yamato and Brun, 2017); and (5) autoclave effects during intrusion (Vrijmoed et al., 2009; Chu et al., 2017) (Fig. 3). In detail, categories 3 and 4 are related, and potentially subcategories of, group 2 models; that is, “deviatoric stress considerations” is the homogenous case whereas the following two model subsets involve heterogeneous complications (i.e., rheology and tectonic settings).

(1) Non-hydrostatic thermodynamics
 Wheeler (2014) argued that differential stress (σ_1 – σ_3) acting on a rock can affect metamorphic reactions, such as shifting the pressures for phase equilibrium boundaries in the *P*-*T* space (i.e., equilibrium lines). Differential stress influences diffusion processes such as diffusion creep or pressure solution, and therefore the usual assumption of a hydrostatic stress state for metamorphic mineral reactions may not be valid. This model depends on the operative grain-scale reaction pathway (Fig. 3A), such that some reactions may be more influenced by differential stress than others (Wheeler, 2014, 2018). Mineral dissolution and reprecipitation (shown schematically between green and pink minerals in Fig. 3A) may follow pathways from high stress to low stress (i.e., pressure solution for the same mineral or incongruent pressure solution for the dissolution of several minerals and precipitation of new minerals), low to high stress (i.e., force of crystallization), or directly across grains as local chemical exchange. These considerations semi-quantitatively suggest ~50 MPa differential stress can offset a mineral reaction by as much as ~500 MPa (Fig. 2 in Wheeler, 2014).

However, this concept does not appear to successfully reproduce experimental data of Hirth and Tullis (1994) (see Tajčmanová et al., 2015), and the impact of non-hydrostatic equilibrium calculations has been questioned (Fletcher, 2015; Hobbs and Ord, 2015). Tajčmanová et al. (2015) suggested that hydrostatic considerations should still be applied to specific mineral reactions because although pressure may vary significantly, the differential stress is rather small at the grain scale (e.g., Tajčmanová et al., 2014).

(2) Deviatoric stress

The simplification that the mean stress, or pressure (*P*), a rock experiences at depth (*z*) is $P = \rho gz$, where *g* is gravitational acceleration and ρ is overlying rock density, assumes no deviatoric stresses (e.g., Gerya, 2015) and no strength (differential stress, σ_1 – σ_3 , equals zero). In detail, this assumption is incorrect, as evidenced by the presence of topography and rock deformation caused by deviatoric stress, including development of folds, faults, foliations, crystallographic and shaped preferred orientations, and mineral rotation fabrics (Moulas et al., 2013, 2019; Schmalholz et al., 2014). Pettrini and Podladchikov (2000) and subsequent papers showed that for a contractional setting (subvertical $\sigma_3 = \rho gz$; Fig. 3B), using some simple assumptions (i.e., $\sigma_2 =$ mean stress and a Byerlee-type yield envelope where ϕ is the angle of internal friction), the effective pressure is given by

$$P_{\text{eff}} = \frac{\rho gh}{1 - \sin(\phi)} \tag{1}$$

Assuming $\phi=40^\circ$, $P_{\text{eff}} = \sim 2.8 \times \rho gh$, thus implying that a pressure estimate might be 2.8 × lithostatic pressure. Alternatively, internal friction of $\phi=30^\circ$ yields $P_{\text{eff}} = \sim 2 \times \rho gh$. The following two categories are related to this deviatoric stress model, where external variables such as rheology or tectonic setting impact the deviatoric stress field.

(3) Strength contrasts

Viscosity heterogeneities in a viscous shear zone imply different rock strengths and different effective pressures (i.e., mean stress). This has been explored in a number of numerical and analytical solutions (e.g., Schmalholz and Podladchikov, 2013; Moulas et al., 2014, 2019). Assuming the rocks are under the same applied stress conditions, the mean stress (pressure) of a stronger phase (blue Mohr circle in Fig. 3C) will be lower than the mean stress of a weaker phase (red Mohr circle in Fig. 3C). This is because the stronger phase has a greater differential stress than the weaker phase. Assuming the two rocks share a common point at their bounding interface, where shear and normal stresses are equal, the mean stress or pressure for each phase will differ. Depending on the orientation, the two rocks may be tied to a common principle stress, such as σ_1 , but this is not required (e.g., Moulas et al., 2014). This will result in a departure from lithostatic pressures.

(4) Tectonic mode switching

During contraction, lithostatic overburden (ρgz) is parallel to a subvertical σ_3 , and if the tectonic regime switches to extension, σ_1 becomes subvertical and thus parallel with ρgz (Yamato and Brun, 2017). Pressure during contraction (P_c) will be greater than the pressure during extension (P_e), which is dictated by rock strength and friction parameters (Fig. 3D). Yamato and Brun (2017) used this tectonic mode switching to explain observations of rapid nearly isothermal pressure drops and decompression following high pressure metamorphism. From a global compilation of high-pressure data, they observed a strong linear relationship between peak pressure and the isothermal pressure drop, which they argued may reflect tectonic mode switching rather than exhumation.

(5) Autoclave

Volume expansion accompanying partial melting and density (ρ) reduction within a relatively stronger confining space will increase the effective pressure (Vrijmoed et al., 2009). Modeling suggests that <2.5% melt of a granite can yield ~5 kbar overpressure (Chu et al., 2017) (Fig. 3E). Vrijmoed et al. (2009) demonstrated this mechanism to generate >2× overpressure using finite element modeling assuming either

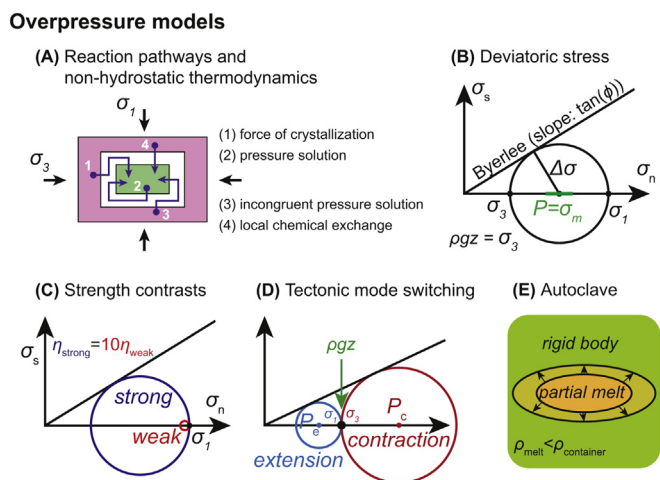


Fig. 3. Generalized models of the five groups of non-lithostatic pressure models discussed in the literature. See text for discussion.

purely elastic or purely viscous behavior. For the viscous case, there is an inverse rate dependence on the modeled overpressure (i.e., slower timescales of partial melting equate to lower maximum overpressure values, all things being equal). These models require the confining vessel/wallrock to be strong enough to resist this inferred pressure increase, and evidence for dikes/veins around regions of partial melting may reflect breaking of the wallrock. Potential failure of the confining container may lead to an observed isothermal pressure drop accompanied by decompression melting and leucosome generation (Vrijmoed et al., 2009). In addition to partial melting, volume-changing metamorphic reactions (e.g., dehydration melting) may drive the autoclave mechanism. To our knowledge, this effect has not been systematically explored via thermomechanical or petrological modeling as a driver for departures from lithostatic pressures (see discussion in Gerya, 2015). The prediction would be that dehydration melting reactions of hydrous phases (e.g., Groppo et al., 2012), such as the breakdown of micas, would increase volume to drive autoclave-related pressure increases. Hydration reactions, when total available fluids are constant, would lead to the opposite effects (e.g., Jones et al., 2015). Dehydration-induced partial melting (e.g., Hallett and Spear, 2014) may together drive increased non-lithostatic pressures.

In this study, we first outline the regional geology of the REWP in northeast Nevada, followed by a review of existing pressure-temperature estimates, which suggest that Neoproterozoic–Paleozoic rocks of Nevada's passive margin stratigraphy were not buried to depths >25 km. Deep burial models are at odds with regional geologic observations, as outlined below, and therefore we propose that non-lithostatic pressure conditions may explain the discrepancy between pressure estimates and field relationships.

3. Background geology of northeast Nevada

East-dipping Mesozoic subduction along the western margin of the North American continent led to the development of the North American Cordillera (e.g., Burchfiel and Davis, 1975; Oldow et al., 1989; Allmendinger, 1992; Burchfiel et al., 1992; DeCelles, 2004; Dickinson, 2004). Retroarc deformation east of the main margin-parallel magmatic arc led to a protracted Jurassic–Paleogene history of contractional deformation across present-day Nevada and Utah, USA (Armstrong, 1968; Royse et al., 1975; Villien and Kligfield, 1986; DeCelles and Coogan, 2006; Zuza et al., 2020). In the Middle–Late Jurassic, plutonism and deformation occurred across the Cordilleran retroarc (e.g., Allmendinger et al., 1984; Oldow, 1984; Thorman et al., 1990, 1992; Miller and Hoisch, 1995; Ketner et al., 1998; Wyld et al., 2003; Rhys et al., 2015; Yonkee et al., 2019; Zuza et al., 2020). The more pervasive and widely recognized phase of contractional deformation and crustal thickening initiated in the Cretaceous, as epitomized by the Sevier fold-and-thrust belt that exists at the roughly longitude of central Utah (Coney and Harms, 1984; DeCelles and Coogan, 2006; Yonkee and Weil, 2015) (Fig. 1A).

Late Cretaceous crustal thickening in the hinterland of the Sevier thrust belt resulted in the construction of the Nevadaplano plateau (DeCelles, 2004; Fig. 1A), which is supported by structural reconstructions (DeCelles and Coogan, 2006), paleoelevation proxies (Cassel et al., 2014), a belt of Late Cretaceous two-mica peraluminous granites interpreted as crustal melts that spans from Canada to Arizona (e.g., Miller and Bradfish, 1980; Lee et al., 2003), elevated Sr/Y ratios from Cretaceous plutons (Chapman et al., 2015), and high pressure (>7 kbar; summarized below in a separate section) metamorphic rocks recorded in the hinterland of this thrust system (e.g., Camilleri and Chamberlain, 1997; Camilleri et al., 1997; Lewis et al., 1999; Cooper et al., 2010; Hallett and Spear, 2014, 2015). The rocks that yielded high pressure estimates were exhumed in the REWP and Snake Range metamorphic core complexes, and are composed of paragneiss and schist whose protoliths were originally the lower part of the Neoproterozoic–Permian sedimentary rocks of western North

America's passive margin. Most stratigraphic thickness estimates for this entire passive margin sedimentary section in eastern Nevada are ~12–15 km (e.g., Stewart and Poole, 1974; Coats, 1987; Colgan et al., 2010), equating to approximately 3–4 kbar of lithostatic pressure for the lowermost rocks (density, $\rho \sim 2.7 \text{ g/cm}^3$). The lower two stratigraphic units are the Neoproterozoic–Cambrian Prospect Mountain Quartzite at stratigraphic depths of ~8 km (~2.1 kbar) and the underlying Neoproterozoic McCoy Creek Group that extends the section down to ~15 km depth (~4 kbar) (Misch and Hazzard, 1962).

Given these stratigraphic constraints, metamorphic pressure estimates of 6–8+ kbar have been used to argue that the rocks were buried more than twice their stratigraphic depths to achieve their recorded pressures (Hodges et al., 1992; Camilleri and Chamberlain, 1997; Lewis et al., 1999; McGrew et al., 2000; Hallett and Spear, 2014, 2015). Camilleri and Chamberlain (1997) hypothesized that an enigmatic thrust fault, known as the Windermere thrust, duplicated the Neoproterozoic–Paleozoic stratigraphic section to bury rocks in the REWP by 2–3× stratigraphic thicknesses in the Late Cretaceous. Lewis et al. (1999) similarly suggested that cryptic crustal shortening around the northern Snake Range (Fig. 1A) buried the Neoproterozoic–Cambrian Prospect Mountain quartzite to 3× stratigraphic depth. For both the REWP and northern Snake Range, there is no direct field evidence for such structures, potentially because they were reactivated and/or obscured during Cenozoic extension (e.g., Camilleri et al., 1997; Wells, 2018). Herein, we focus specifically on the REWP core complex, but emphasize that the similarities between the REWP and northern Snake Range metamorphic core complexes suggests similar phenomena.

Another relevant observation relates to the depth of Eocene gold mineralization in northeast Nevada. The Long Canyon deposit was recently discovered and is an economically important gold deposit in the eastern Pequoop Mountains (e.g., Bedell et al., 2010; Smith et al., 2013). The deposit is located at the base of Ordovician strata in the hanging wall of the Jurassic Independence thrust, which duplicates ~2–3 km of stratigraphy. Its structural depth during Eocene mineralization depends on whether there was deep overthrust burial. Deep burial by a Windermere thrust panel predicts mineralization at depths >10–15 km. Conversely, just accounting for Jurassic Independence thrusting and erosion (e.g., Zuza et al., 2019a, 2020) mineralization would have occurred at a structural depth of ≤5 km, possibly ≤3 km.

4. Geologic restoration of the REWP

The REWP consists of several north-trending ranges in northeast Nevada that share similar rock types and tectonic histories (Figs. 1 and 2). These ranges include, from west to east respectively, the Ruby Mountains, East Humboldt Range, Wood Hills, and Pequoop Mountains (Fig. 2). These ranges were part of the footwall of a west-directed normal fault system that probably started in the Oligocene–Miocene (e.g., Snoke, 1980; Wright and Snoke, 1993; Henry et al., 2011), although argon thermochronology and decompression paths derived from *P-T-t* estimates have been used as evidence for earlier Late Cretaceous exhumation (e.g., Camilleri and Chamberlain, 1997; McGrew et al., 2000; Hallett and Spear, 2015). The rocks in the Ruby Mountains–East Humboldt Range to the west are more strongly deformed than those in the Pequoop Mountains to the east, primarily due to pervasive variable composition intrusions (e.g., mostly leucogranite, quartz diorite, and monzogranite; Lee et al., 2003; McGrew and Snoke, 2015) of Late Cretaceous through Oligocene sills and dikes that are variably deformed by Mesozoic contraction and Cenozoic extension. Accordingly, we have argued that the less pervasively deformed rocks to the east (i.e., the Wood Hills and Pequoop Mountains) are useful for interpreting the history of the REWP (Zuza et al., 2020). For example, the Ruby Mountains–East Humboldt Range typically contain >2/3 intrusions (e.g., Lee et al., 2003; Howard et al., 2011; McGrew and Snoke, 2015), which makes resolving stratigraphic or structural relationships ambiguous. In this section, we schematically demonstrate

how the ranges may have fit together prior to their Cenozoic dismemberment. This restoration is based on existing geologic maps and our own new mapping of the East Humboldt Range and Pequop Mountains.

First, we partially close the intervening basins to approximate Cenozoic Great Basin extension (Fig. 1B), which averages ~50% extension and locally >100% extension (McQuarrie and Wernicke, 2005; Long, 2019). Next, motion on the Pequop normal fault can be restored (Fig. 2), which places the Pequop plate (i.e., the hanging wall of the Pequop fault) to the east-southeast (Zuza et al., 2018, 2020). For this restoration, Pennsylvanian–Permian rocks in the Pequop plate are positioned along strike of similar strata in the southern Pequop Mountains. Note that the thrust relationships observed in the Pequop plate satisfactorily restore along the pseudo-trace of the Independence thrust (e.g., Camilleri and Chamberlain, 1997). A final validation of this restoration comes from the fact that mylonitic lineations in the Ruby-East Humboldt Range suggest top-to-NW (~290° directed) transport, and our restoration of the Pequop plate follows a subparallel vector (Fig. 2). This predicts that the Pequop normal fault is related and parallel to the main mylonitic shear zone in the Ruby-East Humboldt Range.

In our restored framework, we see how the REWP ranges are spatially related. This restoration suggests that the Neoproterozoic–Cambrian strata exposed along the western Pequop Mountains are the same as those in the Wood Hills, consistent with earlier mapping by Thorman (1962, 1970) that demonstrated Paleozoic rocks in the eastern Wood Hills are identical to the western Pequop Mountains. The garnet-in and tremolite-in metamorphic isograds in the westernmost Pequop Mountains correspond to those mapped in the Wood Hills (Camilleri

and Chamberlain, 1997; Wills, 2014; Zuza et al., 2020). There is no major structure between the Wood Hills and Pequop Mountains, beyond the west-dipping high-angle normal faults located along the western flank of the Pequop Mountains, which accommodated eastward tilting of the Pequop Mountains (Zuza et al., 2018). Therefore, the Wood Hills and western Pequop Mountains represent similar structural levels (Fig. 2). In this restored framework we discuss the available pressure-temperature data from the REWP below.

5. Pressure-temperature estimates

In this section, we review available published pressure estimates relevant to this study (Fig. 5; Table 1). First, we focus on aluminum-in-hornblende pressure estimates (e.g., Miller and Hoisch, 1995) from Late Jurassic plutons that intruded Cambrian stratigraphy. This establishes initial depth/burial conditions preceding Late Cretaceous metamorphism and any related deep burial. Then we present Late Cretaceous peak-pressure estimates from the REWP. Lastly, we briefly review available pressure estimates from the northern Snake Range, noting the debate regarding burial depth in the northern Snake Range is very similar to the REWP.

5.1. Late Jurassic pressures

Regionally, in northeast Nevada east of the Roberts Mountain thrust and the city of Ely, NV (Fig. 1A), passive margin stratigraphy was not tectonically buried prior to the Mesozoic. Thus, any lithostatic pressures

Table 1
Compiled pressure –temperature estimates from metamorphic core complexes in eastern Nevada.

Range	Unit	Reference	Age*	Pressure (kbar)	Unc. (kbar)	Temp. (°C)	Unc. (°C)	Geothermal Gradient (°C/km)	Approx. strat. Depth (km)	P_L (kbar)	P_{LT} (kbar)	Ratio P/P_L P/P_{LT}	
Central Ruby Mountains	McCoy Creek	Hudec (1992)	Late Cretaceous!	4.1	1	600	50	39	12	3.2	4.2	1.3	1.0
Central Ruby Mountains	McCoy Creek	Hudec (1992)	Jurassic	3.2	1	495	50	41	13	3.4	4.5	0.9	0.7
Central Ruby Mountains	McCoy Creek	Jones (1999)	Late Cretaceous	4.3	1	525	50	33	12	3.2	4.2	1.3	1.0
East Humboldt Range	McCoy Creek	Hurlow et al. (1991)	Cenozoic	3.5	1	600	50	45	12	3.2	4.2	1.1	0.8
East Humboldt Range	Graphite Schist/Paragneiss	Hallett and Spear (2014, 2015)	Late Cretaceous	9.5	1	700	50	19	13	3.4	4.5	2.8	2.1
East Humboldt Range	Garnet paragneiss/migmatitic schist	Hallett and Spear (2014, 2015)	Late Cretaceous	7.0	1	700	50	26	13	3.4	4.5	2.0	1.6
East Humboldt Range	McCoy Creek	Hodges et al. (1992)	pre-Late Cretaceous	10.3	0.5	525	50	14	12	3.2	4.2	3.2	2.4
East Humboldt Range	McCoy Creek	Hodges et al. (1992)	Late Cretaceous	6.0	0.5	587	50	26	12	3.2	4.2	1.9	1.4
Northern East Humboldt Range	Metapelite (deeper levels)	McGrew et al. (2000)	Late Cretaceous	7.5	1.5	675	50	24	13	3.4	4.5	2.2	1.7
Northern East Humboldt Range	Metapelite (shallower)	McGrew et al. (2000)	Late Cretaceous	7.0	1	675	50	26	13	3.4	4.5	2.0	1.6
Wood Hills	Dunderburg Shale	Hodges et al. (1992)	Cretaceous	6.0	1	575	50	25	7	1.9	2.9	3.2	2.1
Wood Hills	Dunderburg shale	Wills (2014)	Late Cretaceous	6.3	1	630	50	26	7	1.9	2.9	3.6	2.3
Pequop Mountains	Prospect Mountain	This Study	Late Cretaceous	7.0	1	550	50	21	8	2.1	3.2	3.3	2.2
Pequop Mountains	Geologic constraint	Zuza et al. (2018, 2019a)	Jurassic	2.8	1	500	50	48	8	2.1	3.2	1.3	0.9
Northern Snake Range	McCoy Creek	Lewis et al. (1999)	Cretaceous	8.1	0.7	610	50	20	12	3.2	4.2	2.6	1.9
Northern Snake Range	McCoy Creek	Cooper et al. (2010) [®]	Cretaceous	6.1	0.75	550	50	24	12	3.2	4.2	1.9	1.4
Northern Snake Range	McCoy Creek	Cooper et al. (2010) [®]	Cretaceous	8.1	0.7	610	50	20	12	3.2	4.2	2.6	1.9

Notes: P_L is lithostatic pressure; P_{LT} is lithostatic pressure with 4 km of thickening assumed.

* As specified in reference; ! Reinterpreted as Late Cretaceous by Jones (1999).

[®] Broad average of two datapoints.

experienced by these units should be related to stratigraphic depth. Late Jurassic deformation, as part of the Elko Orogeny, affected much of northeast Nevada (e.g., Thorman et al., 1990, 1992; Miller and Hoisch, 1995; Zuza et al., 2020). To quantify this deformation and tectonic burial, Miller and Hoisch (1995) presented aluminum-in-hornblende pressure estimates for Middle–Late Jurassic plutons in northeast Nevada. The aluminum-in-hornblende barometry method has been criticized as unreliable (e.g., Pattison and Vogl, 2005). However, it is our view that successful applications of these techniques, such as in the Sierra Nevada (e.g., Nadin et al., 2016), Searchlight pluton of southern NV (Bachl et al., 2001; Zuza et al., 2019c), and Gangdese batholith of Tibet (Cao et al., 2020), demonstrate that careful treatment and evaluation of the samples can yield meaningful insights of emplacement pressures. These above cited examples show reasonable pressure trends that are corroborated by external constraints, such as nearby wallrock pressures, palinspastic reconstructions, presence/absence of magmatic epidote indicative of medium-high pressures (e.g., Ghent et al., 1991), or relationship with copper porphyry deposits (i.e., shallow depths of 1–5 km) (e.g., Cao et al., 2020). In light of these considerations, we assume that the aluminum-in-hornblende method is a useful technique when applied carefully. Our main interpretations of this study are not based on these datapoints, but they provide useful constraints on the geologic record prior to attainment of inferred prograde peak pressures.

Plutons in northeast NV consistently yield pressures of 3–4 kbar (Miller and Hoisch, 1995). Most relevant to this study, the Jurassic Silver Zone Pass pluton in the Toano Range intruded middle Cambrian strata (SZP in Fig. 1B) and yielded a pressure estimate of 3.3 ± 0.5 kbar using the Johnson and Rutherford (1989) calibration. We analyzed a new sample from Silver Zone Pass to verify the Miller and Hoisch (1995) results. Methods and data are in the Supplemental Materials, and we obtained a similar pressure estimate of 3.1 ± 0.5 kbar using the Mutch et al. (2016) calibration. We reprocessed the Miller and Hoisch (1995) data with the same calibration and obtained 3.6 ± 0.5 kbar, which overlaps our estimate within uncertainties.

These observations indicate that middle Cambrian strata intruded by the Jurassic Silver Zone Pass pluton were at depths of ~ 3.1 – 3.6 kbar at this time, or ~ 12.5 km. This is ~ 1 kbar higher pressures than expected for stratigraphic depths, which has been used as evidence to suggest Middle–Late Jurassic crustal shortening and thickening on the order of ~ 3 – 4 km, just prior to post-kinematic pluton intrusion (Miller and Hoisch, 1995). Alternatively, we acknowledge that ~ 1 kbar differences may not be significantly resolvable by the method, in which case we may conservatively interpret that these datapoints simply convey that Cambrian rocks were at or near stratigraphic depths in the Middle–Late Jurassic. New detailed geologic mapping has documented a Late Jurassic-aged ramp-flat thrust fault with 2–3 km unit duplication in the Pequop Mountains (e.g., Zuza et al., 2018, 2019a, 2020), which is consistent with the aluminum-in-hornblende barometry suggesting some minor burial.

In the central Ruby Mountains, Hudec (1992) estimated similar pressures from andalusite-bearing McCoy Creek Group rocks (Fig. 1B). These rocks were crosscut by the ca. 153 Ma Dawley Canyon pluton, which led Hudec (1992) to interpret that the McCoy Creek Group was at ~ 3 kbar in the Middle–Late Jurassic. An overprinting slightly higher grade metamorphic event was interpreted by Hudec (1992) as occurring in the Late Jurassic. However, Jones (1999) subsequently reinterpreted this second phases of metamorphism as Late Cretaceous and thus this event is discussed later in the “Late Cretaceous pressures” section. The Eocene Harrison Pass pluton intruded just (≤ 5 km) south of these localities, and aluminum-in-hornblende pressure estimates yielded similar ~ 3 kbar (Barnes et al., 2001).

In summary, available pressure estimates and field evidence imply a minor phase of Late Jurassic crustal thickening. This suggests that if minor Jurassic strain is preserved in the rock record, one would expect that any postulated significant Late Cretaceous shortening and unit duplication should be observable in the field relationships.

5.2. Late Cretaceous pressures

Fig. 1E shows existing pressure estimates for rocks along a west-east traverse across the REWP (summarized in Table 1). Available datasets were compiled from works spanning several decades and involving different methods, including traditional exchange thermometers and net transfer reaction barometry (Hurlow et al., 1991; Hudec, 1992; Hodges et al., 1992; Jones, 1999; McGrew et al., 2000) and more modern applications of phase equilibrium modeling (Hallett and Spear, 2014; Wills, 2014) (Fig. 2A for map locations). Our proposal of non-lithostatic pressure in this study hinges on the accuracy of pressure estimates from this region. Below we briefly summarize these published estimates but also refer the reader to the original source material. Over the past three decades, these pressures are broadly reproducible from different authors and widely cited (e.g., see compilation of Henry et al., 2011).

High pressures at moderate temperatures in the East Humboldt Range are evidenced by local and/or relict presence of kyanite + staurolite + garnet + biotite, which may have been attained in the Late Jurassic or Cretaceous (e.g., Snoke, 1992; McGrew et al., 2000; Henry et al., 2011). More common assemblages of garnet + sillimanite + biotite are interpreted as higher temperature Late Cretaceous peak metamorphism (McGrew et al., 2000). McGrew et al. (2000) employed Thermocalc (Powell and Holland, 1988) on mostly metapelite samples (14 metapelites and 2 metabasite) collected from across the East Humboldt Range with assemblages of biotite + sillimanite + garnet + quartz + plagioclase \pm chlorite \pm muscovite \pm K-feldspar \pm rutile \pm ilmenite. From sixteen samples from different structural levels, McGrew et al. (2000) obtained estimates spanning 5–9 kbar and 600–700 °C (Figs. 2A and 5A).

More recently, in coupled comprehensive geochronology-thermobarometry studies, Hallett and Spear (2014, 2015) obtained similar peak *P-T* results for Late Cretaceous metamorphism on similar rock types. These two studies provided detailed mineral chemistry and zoning constraints, which were incorporated with thermobarometry calculations and thermodynamic modeling. Temperatures were estimated via the garnet-biotite Fe–Mg exchange (GARb; e.g., Ferry and Spear, 1978; Hodges and Spear, 1982) and Zr-in-rutile thermometers (e.g., Watson et al., 2006; Tomkins et al., 2007). Pressures were estimated by the garnet-muscovite-plagioclase-biotite (GASP; Hodges and Crowley, 1985), garnet-hornblende-plagioclase-quartz (GHPQ), and garnet-plagioclase-muscovite-biotite (GPMB) barometers (Hodges and Spear, 1982; Powell and Holland, 1988). In Table 1 and Fig. 5, we report only estimates of peak pressure conditions, at 7–9.5 kbar and ~ 700 °C. Thermodynamic modeling was conducted using assumed bulk compositions in the MnNCKFMASH(\pm Ti) system, and yielded overlapping estimates to the aforementioned thermobarometry results (Hallett and Spear, 2014). Zircon and monazite dating confirm a Late Cretaceous age for prograde peak metamorphism, with rare Jurassic monazite ages suggesting an earlier phase of metamorphism (Hallett and Spear, 2015).

Just east of the main East Humboldt Range in Clover Hill (Fig. 2A), Hodges et al. (1992) used conventional thermobarometry on samples of the McCoy Creek Group—i.e., GARb (e.g., Ferry and Spear, 1978; Hodges and Spear, 1982), GASP (Hodges and Crowley, 1985), and the garnet-rutile-aluminosilicate-ilmenite barometer (GRAIL e.g., Bohlen et al., 1983)—and Gibbs method modeling (Spear and Selverstone, 1983) to calculate high pressures of 6–10 kbar. These samples contain kyanite that was pre-kinematic with respect to the dominant schistosity defined by sillimanite + muscovite + biotite (Hodges et al., 1992). Just east in the Wood Hills, the same methodology employed on Cambrian Dunderberg Shale samples with garnet + staurolite \pm kyanite yielded peak pressure estimates of ~ 6 kbar at ~ 575 °C (Hodges et al., 1992; Fig. 2A). On this Cambrian Dunderberg Shale unit, Wills (2014) conducted phase equilibrium modeling, GASP-GARb thermobarometry, and the Gibbs method to estimate pressures of 6–7 kbar at

600–700 °C (Figs. 2A and 5A). We report in Table 1 and Fig. 5 the approximate mean *P-T* values from Wills (2014)'s final model paths.

A series of relatively lower pressure estimates in the REWP were all derived from Neoproterozoic McCoy Creek Group. Hurlow et al. (1991) aimed to document pressures of metapelite mylonitization in the central East Humboldt Range. This study documented a pre-mylonite mineral assemblage of sillimanite + K-feldspar + muscovite + quartz with a synkinematic quartz + biotite + muscovite + plagioclase. Quantitative thermobarometry via GARB thermometry (Ferry and Spear, 1978; Hodges and Spear, 1982) and GASP barometry (Ghent and Stout, 1981; Hodges and Crowley, 1985) yielded ~3.5 kbar at 600 °C (Fig. 2A).

In the central Ruby Mountains, a phase of upper amphibolite sillimanite-grade metamorphism overprinted the Late Jurassic record, evidenced by mineral texture relationships, as reported by Hudec (1992). Jones (1999) studied similar rocks in the central Ruby Mountains, and interpreted this later phase as a Late Cretaceous based on co-incident garnet + sillimanite observed in Late Cretaceous pegmatitic leucogranite (Table 1). Therefore, we discuss Late Cretaceous pressure estimates from Hudec (1992) and Jones (1999) together. The dominant mineral assemblage is muscovite + biotite + plagioclase + sillimanite ± garnet ± cordierite. Hudec (1992) used GEO-CALC software (e.g., Perkins et al., 1986; Brown et al., 1988) to calculate all possible equilibria between relevant phases with compositional inputs for muscovite, biotite, plagioclase, garnet, cordierite, and staurolite. Analysis of 6 samples yielded a cluster of *P-T* results at ~4.1 kbar and ~600 °C. Later, Jones (1999) applied TWQ (e.g., Berman, 1991) to a sample containing quartz + biotite + muscovite + plagioclase + garnet + sillimanite to obtain estimates of ~4.3 kbar and 525 °C.

Herein, we assume that these published pressure estimates are valid. However, there are potential limitations for the aforementioned data. The REWP experienced a polyphase deformation, thermal, and metamorphic history, with apparently distinct punctuated Late Jurassic and Late Cretaceous shortening and burial (e.g., Hudec, 1992; McGrew et al., 2000; Hallett and Spear, 2015; Zuza et al., 2020), various intrusions and reheating events from the Late Jurassic to Miocene (e.g., Henry et al., 2011), and complicated exhumation, decompression, and retrogression (e.g., Hallett and Spear, 2014). Therefore, any burial history and estimated pressures reflect this polyphase history, and require assumptions for equilibrium assemblages. Hallett and Spear (2014, 2015) carefully documented compositional zoning via X-ray mapping of important phases to try to better constrain these assumptions. Related to this, partial melting affected the chemical history of these rocks. For example, Ca zoning in garnet may reflect changes in pressure while garnet and plagioclase are in equilibrium, or incorporation of Ca by garnet as plagioclase breaks down during partial melting (Hallett and Spear, 2014). Therefore, measured Ca concentrations may be impacted by pressure changes, bulk composition changes partial melting, or a combination of complications.

5.3. New Raman inclusion barometry

To supplement these published data, and expand pressure constraints to the east, we conducted Raman inclusion barometry (i.e., QuiG) on quartz inclusions within garnet (e.g., Schmidt and Ziemann, 2000; Kohn, 2014; Angel et al., 2017) from a Neoproterozoic–Cambrian Prospect Mountain Quartzite sample from the western Pequop Mountains (40°55'59.67"N; 114°38'29.55"W; Fig. 2). These methods assume hydrostatic compression of quartz and rely on a shift of the 464 cm⁻¹ Raman band frequency of quartz. We use this method over the recently developed anisotropic Grüneisen tensor method (Angel et al., 2019), which uses data on three modes to assess strain independently on each crystallographic axis. Bonazzi et al. (2019) compared hydrostatic and anisotropic inclusion pressure models, and there was no significant deviation of these methods for pressures <3.0 GPa (e.g., Thomas and Spear, 2018), provided small deviatoric stresses (e.g., Fig. 4a of Bonazzi et al., 2019). Therefore, we use the higher resolution 464 cm⁻¹ peak assuming

hydrostatic compression of quartz. Detailed methods and analyses are in the Supplemental Materials.

The Prospect Mountain sampling locality (Fig. 2A) is the lowermost exposure of a continuous ~7–8-km-thick package of Neoproterozoic through Permian stratigraphy, and the uppermost rocks are entirely undeformed and unmetamorphosed (red dashed box in Fig. 2A). The sample is a quartzite with muscovite-rich partings, sometimes with ~1–2 mm garnet. Quartz grains have a strong shape preferred orientation but no crystallographic preferred orientation. Quartz is recrystallized with lobate interfingering grain boundaries suggesting grain boundary migration recrystallization with more minor subgrain rotation. Based on the quartz microstructures, presence biotite/tremolite in nearby units, and a regional compilation of peak temperature data (e.g., Zuza et al., 2020; Fig. 4), we interpret this sample to have experienced peak temperatures of ~500–550 °C.

We analyzed 21 quartz inclusions in two garnet grains from this sample (Fig. 6; laboratory labels garnet 1 and 3) and wavenumber shifts are plotted in Fig. 6. We interpret that this sample experienced peak temperatures of ~500–550 °C and conservatively assume that prograde garnet growth that entrapped the quartz occurred at ~500 °C. Therefore, we model QuiG pressures using a range of temperatures of 450 °C, 500 °C, and 533 °C, but favor results for the 500 °C model. Nineteen of the analyses yielded similar pressure estimates with two outlier analyses yielding higher pressures. Because there are numerous mechanisms to relax pressures (e.g., Angel et al., 2014; Bonazzi et al., 2019; Zhong et al., 2020), it is common practice to consider and use the higher QuiG pressure estimates. However, due to an imprecise temperature history, the consistency of the 17 other estimates, and in the interest of conservative estimates to compare against geologic reconstructions (i.e., pressure estimates that minimize implied non-lithostatic pressure), we excluded these two highest analyses to determine an average QuiG pressure of 7 ± 1 kbar, assuming 500 °C inclusion entrapment (Fig. 6). Hotter or colder entrapment temperatures would shift pressure estimates to ~7.5 kbar or ~6.2 kbar, respectively (Fig. 6; Supplemental Material). The consistency of these estimates (Fig. 6) gives us confidence in the results, suggesting that inclusion anisotropy or geometry is not significantly influencing this sample, which would predict more variability (e.g., Mazzucchelli et al., 2018; Bonazzi et al., 2019). We interpret that this pressure was attained on a prograde path, and therefore for peak *P-T* we report ~7 kbar at ~550 ± 50 °C in Table 1 (Fig. 5). If lithostatic, this implies burial to ~26 km and a geothermal gradient of ~20 °C/km.

This quartz-in-garnet Raman-based pressure estimate is similar to other relatively high-pressure estimates in the REWP (Fig. 5). Muscovite and biotite ⁴⁰Ar/³⁹Ar thermochronology (Zuza et al., 2019a) suggests that prograde metamorphism occurred in the Late Cretaceous, although our geologic mapping and regional datasets suggest that the Late Cretaceous event overprinted a previous Late Jurassic history (e.g., Thorman et al., 1990, 2019; Zuza et al., 2020). Wills (2014) provided a Lu–Hf garnet age from the Wood Hills to the west of ca. 83 Ma, which we interpret may represent a similar timing of garnet growth in the Prospect Mountain sample analyzed here.

In summary, reported Late Cretaceous pressure estimates from across the REWP tend to fall into two groups: higher pressures of 6–8+ kbar and lower pressures of 3–4 kbar (Fig. 5). Where available, geochronologic constraints suggest that peak pressures for the high pressure data were attained in the Late Cretaceous (e.g., McGrew et al., 2000; Wills, 2014; Hallett and Spear, 2015). If these pressure estimates are lithostatic, they suggest the rocks were buried to 23–30+ km depths ($\rho \sim 2.7$ g/cm³) (Fig. 5), or approximately 2–3 × the thickness of the passive margin section. Conversely, authors interpret the lower pressure estimates to represent mylonitic conditions during range exhumation and normal-sense shearing (e.g., Hurlow et al., 1991). These pressures are generally compatible with lithostatic pressures predicted for McCoy Creek Group rocks that would have been at 10–14 km depth (2.6–3.7 kbar). The across-strike west-east compilation in Fig. 1E shows

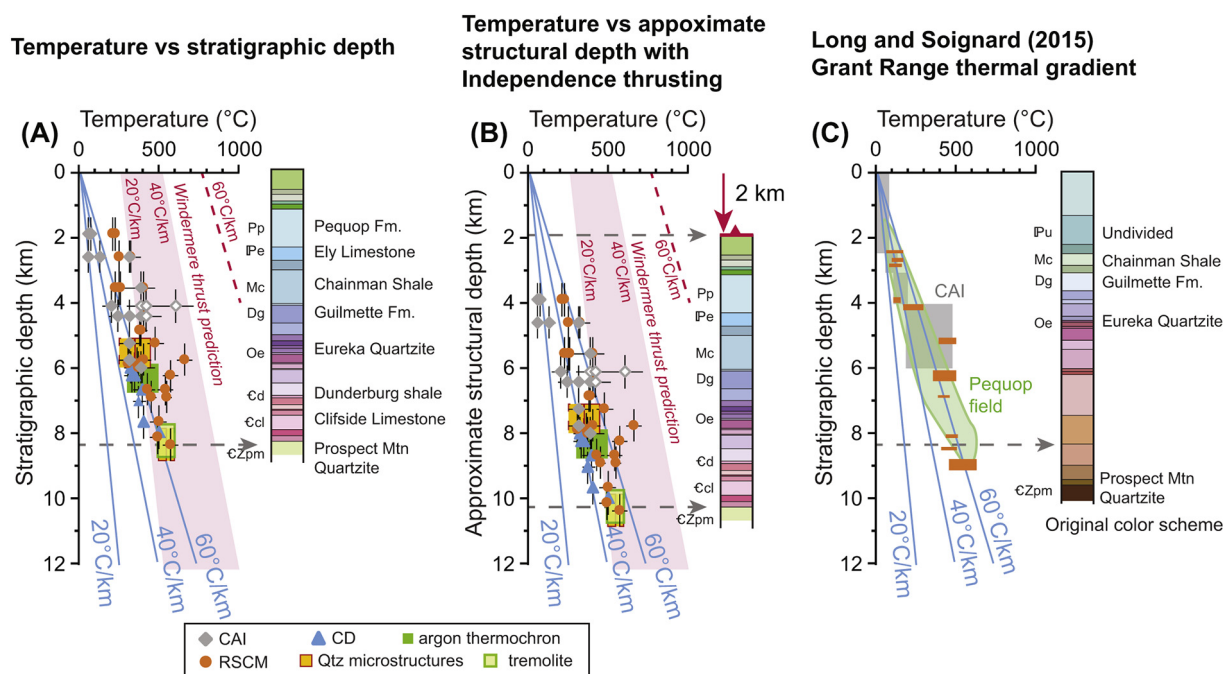


Fig. 4. (A) Stratigraphic depth (0.5 km uncertainty) versus peak-temperature (T_p) across the Pequop Mountains (modified from Zuza et al., 2020). Accompanying stratigraphic column (same vertical scale) shows observed thicknesses (Zuza et al., 2018, 2019a). Only some units are named; the complete stratigraphic column is in Zuza et al. (2020). Data: CAI (Zuza et al., 2020); RSCM (Zuza et al., 2020; Howland, 2016); calcite-dolomite thermometry (CD) (Howland, 2016); quartz recrystallization microstructures (Latham, 2016; this study); argon thermochronology (Zuza et al., 2019a); the presence of metamorphic tremolite (this study). CAI data with white symbol and brown outline are interpreted to have been affected by hydrothermal fluids. Predicted thermal structure assuming Windermere thrust hypothesis is shown in red. (B) Same as Fig. 4A, except that ~2 km thickening is invoked based on mapped Independence thrust relationships; see text. (C) Another example of high geothermal recorded in the Great Basin by Long and Soignard (2016) with their study area shown in Fig. 1A. Their stratigraphic column was drafted to the right of the plot, with orange boxes showing RSCM, vitrinite reflectance, and Rock-Eval pyrolysis analyses. Grey boxes are published CAI constraints from the region (Crafford, 2007) and the green field is a comparison of T_p observations from Fig. 3A against the Long and Soignard (2016) dataset. Note the similar geothermal gradients >40 °C/km. (For interpretation of the references to color in this figure legend, the reader is referred to the web version of this article.)

approximate stratigraphic depths for the analyzed samples, which spanned Cambrian to Neoproterozoic stratigraphy at stratigraphic depths of 8–15(?) km. We also show the approximate range of possible stratigraphic depths assuming ~4 km of structural burial due to known and observed Mesozoic contractional structures (e.g., Jones, 1999; Zuza et al., 2020).

Although pressure estimates from the REWP vary significantly, the estimated temperature range for these same rocks is generally restricted to 500–650 °C (Fig. 5). Accordingly, if the pressure estimates are reliable and represent lithostatic conditions, the high (6–8+ kbar) and low (3–4 kbar) pressure groups can be divided into two broad domains of inferred paleo-geothermal gradients: <20 – 25 °C/km and 40 – 50 °C/km respectively (Fig. 5). In this regard, the higher pressure estimates require relatively low geothermal gradients of ≤ 25 °C/km if pressure corresponds with depth. This represents one key test for lithostatic versus non-lithostatic conditions.

5.4. Northern Snake Range pressures

In the classic northern Snake Range metamorphic core complex (Fig. 1A), gently dipping Neoproterozoic–Cambrian strata (i.e., McCoy Creek Group and Prospect Mountain Quartzite) are strongly mylonitized (e.g., Miller et al., 1983; Lee et al., 2017). The region records top-east normal-sense exhumation of these rocks, with Cambrian–Permian rocks juxtaposed over the Neoproterozoic–Cambrian mylonitic core. Lewis et al. (1999) obtained quantitative pressure estimates from this region on samples containing the mineral assemblage quartz + muscovite + biotite + garnet + plagioclase + staurolite \pm kyanite \pm tourmaline \pm apatite using the GARB exchange thermometer (e.g., Ferry and Spear, 1978; Hodges and Spear, 1982), GASP barometer (Hodges and Crowley, 1985), and GBMP (Powell and Holland, 1988)

from phases interpreted to be in equilibrium. They obtained 8.1 kbar pressure estimates at ~610 °C (yellow box L99 in Fig. 5A) from the McCoy Creek samples. Later work using the GARB thermometer and GMBP barometer on the same rock types confirmed these high pressures, although with some variability (~6–8 kbar) interpreted to represent spatial differences in Mesozoic thrust footwall–ramp geometries (Cooper et al., 2010; F10 boxes in Fig. 5A). Cooper et al. (2010) also presented MnNCKFMASH pseudosections for McCoy Creek samples based on their bulk geochemistry that were consistent with these previous estimates. In summary, the northern Snake Range constraints are very similar to the REWP, including McCoy Creek rocks that would have originated at stratigraphic depths of ~12–15 km that were estimated to have attained pressures of >6 –8 kbar in the Late Cretaceous (Fig. 5).

6. Discussion

6.1. Predictions of deep tectonic burial

If peak metamorphic pressures are lithostatic, the 6–8+ kbar pressure estimates from the REWP (Fig. 5) suggest burial of the Neoproterozoic–Paleozoic stratigraphy to depths >20 –25 km. From these estimates, there are three possible inferences: (1) the pressures were estimated incorrectly due to complications of mineral equilibrium, polyphase metamorphism, reaction overstepping (e.g., Pattison et al., 2011; Spear, 2017; Spear and Pattison, 2017), or other factors and the local rocks were never deeply buried; (2) the pressures can be satisfactorily converted to lithostatic depths and reflect deep Mesozoic burial (i.e., the deep burial model); or (3) the pressures are generally accurate but are non-lithostatic pressures resulting from one or several overpressure mechanisms (i.e., the overpressure model). Regarding point one, we argue that numerous workers over the past three decades have

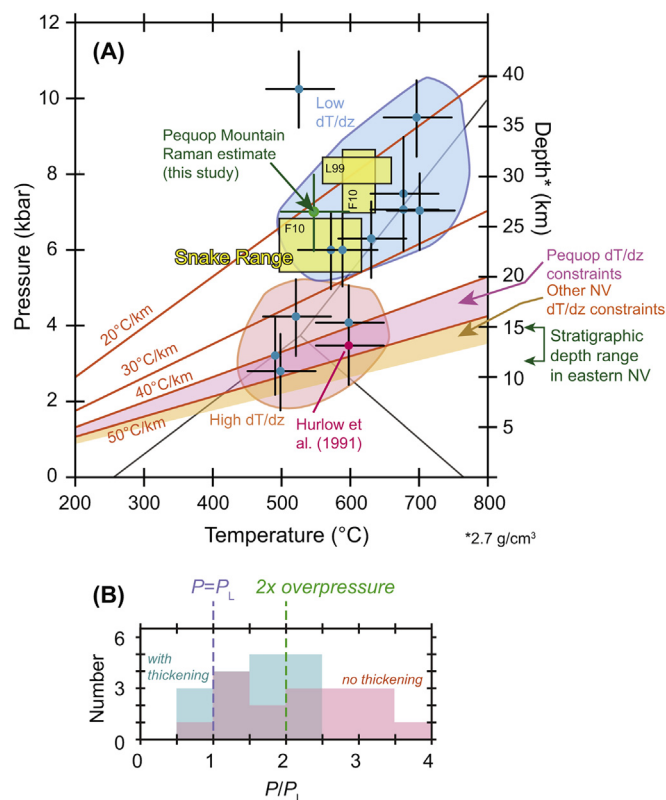


Fig. 5. (A) Compilation of available pressure-temperature data from the REWP, contoured by geothermal gradient assuming a crustal density of 2.7 g/cm³. Data discussed in text and in Table 1. Almost all data is from the REWP, but yellow boxes are from the northern Snake Range (L99—Lewis et al., 1999; F10—Cooper et al., 2010). Note that the data defines two populations: the higher pressure samples suggest normal geothermal gradients (20–25 °C/km), whereas the lower pressure estimates suggest an elevated geothermal gradient (>30–40 °C/km). Pink shading highlights Cretaceous thermal gradient (dT/dz) calculated for the Pequop Mountains (i.e., Fig. 4 and Zuza et al., 2020) and orange shading defines geothermal gradients determined by Miller and Gans (1989), Long and Soignard (2016), and Long et al. (2018). The Hurlow et al. (1991) datapoint is highlighted in red because it is discussed in detail in the text. Green stratigraphic depth arrows show expected depth of Cambrian–Neoproterozoic rocks. (B) Histogram of observed pressure estimates against inferred lithostatic pressure (P/P_L) for the data in Fig. 5A. Blue bars involve ~4 km structural thickening within the REWP, such that ~4 km is added to the P_L value for the stratigraphic depth of a pressure-estimate sample, thus lowering the P/P_L ratio. This is a reasonable assumption as discussed in the text. Pink boxes include no thickening. Data compiled in Table 1. Note that the “with thickening” data cluster between no overpressure ($P/P_L = 1$) and 2× overpressure ($P/P_L = 2$). (For interpretation of the references to color in this figure legend, the reader is referred to the web version of this article.)

published consistent pressure estimates using a variety of methods, as outlined above, resulting in pressures that cluster at 6–8 kbar (Fig. 5). If these pressures are not accurate, then many pressures reported globally (e.g., Brown et al., 2020) would need reevaluation. Here we do not intend to suggest that.

Options 2 versus 3 correspond to models of deep burial versus overpressure, which we test with the geologic record of the REWP. Specifically, a deep-burial hypothesis makes specific predictions for the lateral continuity of thrust faults and burial magnitude, timing of metamorphism and anatexis, initial depth of the Long Canyon Carlin-type gold deposit, and magnitude/timing of Cenozoic extension to exhume the rocks. These model predictions are summarized in Table 2 and expanded on below.

Deep burial predicts major thrust faults with large stratigraphic separations. These faults may potentially be covered or obscured by later Cenozoic extension. Within the North American Cordillera, this deep burial and/or significant overthrusting is concentrated in small pockets,

such as the REWP and northern Snake Range. In between these regions, contractional strain and tectonic burial/duplication is significantly less. The deep burial models predict relatively low geothermal gradients (≤ 25 °C/km), whereas overpressure models require high temperature gradients (40–50 °C/km).

The voluminous Late Cretaceous melts in the REWP (e.g., Lee et al., 2003; Howard et al., 2011) have been postulated to be genetically related to significant crustal shortening and thickening. Deep burial models suggest that the melts were generated as McCoy Creek Group pelites were tectonically buried, and thus prograde metamorphism should precede voluminous in-situ melting and intrusions. The overpressure model suggests that a high geothermal gradient, driven from an external source and/or heat advection from melting at depth, melted pelites at shallower (nearly stratigraphic) depths via dehydration melting. Long and Soignard (2016) showed shallow crustal metamorphism in the Grant Range and highlighted the efficiency of Late Cretaceous magmatism in heating the middle-upper crust (Fig. 1A). Ti-in-zircon thermometry suggests that Late Cretaceous two-mica melts were generated at ~600–700 °C (Hallett and Spear, 2015), which is similar to other peraluminous granites, including the Arunachal leucogranites in the Himalaya (Harrison and Wielicki, 2016). Therefore, deep burial models suggest that McCoy Creek Group pelites were melted at depth with a relatively low thermal gradients, whereas overpressure models require a hot geothermal gradient to melt the pelites at shallower depths. Dehydration melting of pelites could occur as shallowly as 12–14 km with high thermal gradients in eastern Nevada (Long and Soignard, 2016). There is a well-established belt of Late Cretaceous peraluminous granites stretching from Arizona to Canada (Miller and Bradfish, 1980), and there is not evidence for significant thrust burial across this entire domain (e.g., Crafford, 2007; Van Buer et al., 2009; Long, 2012, 2015). Deep REWP burial models imply that the REWP leucogranites are distinct from other peraluminous rocks in the two-mica belt because they were formed specifically as a result of local crustal thickening.

The depth of Eocene gold mineralization at Long Canyon, in the Pequop Mountain (Fig. 2), provides another test of burial models. Deep burial models that invoke the pre-Cenozoic Windermere thrust panel(s) suggest mineralization at depths >10–15 km, whereas just accounting for Jurassic Independence thrusting and erosion (e.g., Zuza et al., 2019a, 2020) suggests mineralization at a structural depth of ≤ 5 km. Robust constraints on the timing and magnitude of Cenozoic extension can also elucidate burial depth. Deep burial requires constrained extension magnitudes to be sufficient to exhume rocks from ~30 km depth. Tectonics models favoring deep burial rely on some component of late Cretaceous or early Cenozoic exhumation (McGrew et al., 2000; Hallett and Spear, 2014, 2015), whereas Miocene-to-present extension can exhume rocks from stratigraphic depths to the surface on mapped normal faults and rotated blocks (e.g., Colgan and Henry, 2009; Colgan et al., 2010; Henry et al., 2011; Zuza et al., 2020).

6.2. Testing deep burial versus overpressure models

We suggest that available geologic constraints are at odds with deep burial (Table 2), and therefore propose that non-lithostatic overpressure caused the relatively high pressures observed in the REWP. Field relationships from decades of geologic mapping (e.g., Thorman, 1962, 1970; Henry and Thorman, 2015; Zuza et al., 2018, 2019a) do not suggest any high magnitude crustal shortening or larger stratigraphic separation. The ~7 kbar pressure estimate obtained in this study from the Prospect Mountain quartzite is from the base of a continuous ~7–8-km-thick stratigraphic section up to undeformed and unmetamorphosed Permian strata (red dashed box in Fig. 2A) (Zuza et al., 2020). If the Prospect Mountain quartzite was buried to >25 km depth, it follows that the upper Permian rocks from this continuous section would have also been buried and deformed. This is not observed.

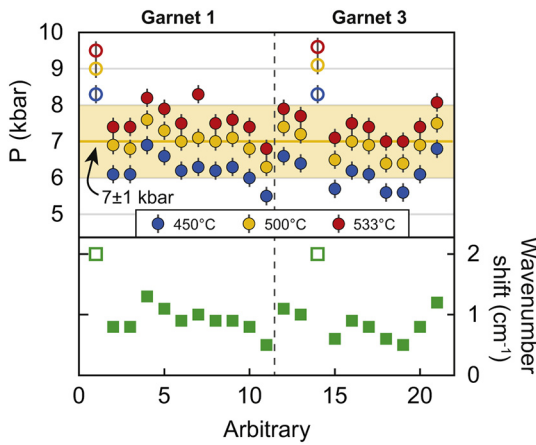


Fig. 6. Raman inclusion barometry results, including wavenumber shifts and modeled pressures for two analyzed garnets (i.e., garnets 1 and 3) assuming three temperatures (450 °C, 500 °C, and 533 °C). Methodology discussed in the text (e.g., Schmidt and Ziemann, 2000; Kohn, 2014; Angel et al., 2017). Analyses cluster around an average pressure of ~7 kbar; open symbols are two outlier analyses that were excluded from the mean. Note that the yellow shading is our reported 7 ± 1 kbar value, which encompasses most analyses at the three modeled temperatures.

However, the Independence thrust in the Pequop Mountains has 2–3 km stratigraphic separation and is a clearly visible and mappable structure (Camilleri, 2010; Zuza et al., 2018, 2020). In the Ruby Mountains-East Humboldt Range, probable Neoproterozoic McCoy Creek Group rocks are observed structurally above Neoproterozoic-Cambrian Prospect Mountain Quartzite (e.g., Howard, 2000), which also implies unit repetition on the order of kilometers. This region is so pervasively intruded that unit assignments of monotonous quartzite-rich rocks is nonunique and open for interpretation. Regardless, the hypothesized Windermere thrust must have been much larger, and it apparently left no surface trace. If real, this structure must have been completely obscured by later Cenozoic extension, with an example normal fault drafted on the model cross sections of Fig. 1C and D. The hanging wall of the Cenozoic extension would have been massive to (1) completely remove the thickness of the overlying Windermere thrust, and (2) remove any trace of high-magnitude pre-Cenozoic shortening. This required high-magnitude extension is at odds with extension observations and crustal thickness to the west of the REWP, as discussed in Colgan and Henry (2009).

The character of this proposed thrust system is entirely different from anything observed in the eastern Great Basin. Clear examples of confirmed hinterland thrust faults include those near Eureka, NV (Long et al., 2014, 2015), in the White Pine Mountains (Humphrey, 1960; Gans, 2000), and the Confusion Range in western Utah (Greene, 2014). These structures fit within the three large synclinoria (and bounding anticlinoria) located near the Nevada-Utah border (Fig. 1A)

(e.g., Hose and Blake, 1976; Gans and Miller, 1983; Welch et al., 2007; Long 2012, 2015; Greene, 2014). These types of features are observed in regional compilations of erosion levels beneath Cenozoic rocks (Armstrong, 1968; Gans and Miller, 1983; Van Buer et al., 2009; Long, 2012), which conversely show no erosional evidence of any proposed major overthrust or intracontinental subduction system anywhere near REWP or to the south. In summary, the Windermere thrust hypothesis envisions a thrust system that is atypical of the Cordillera and at odds with geology of the eastern Great Basin. Below we discuss how this envisioned structure is dissimilar to other structures observed globally in orogenic plateaus.

The deep burial models require a low geothermal gradient of ≤ 25 °C/km. We argue that this low value is unlikely because (1) the Late Cretaceous paleo-geothermal gradient observed in the Pequop Mountains was 40–50 °C/km (Fig. 4A and B) (Thorman et al., 2019; Zuza et al., 2020); (2) further afield estimates of Mesozoic thermal gradients in the eastern Great Basin are all high (≥ 40 °C/km) and the Nevadaplano involved a classically hot retroarc (e.g., Miller and Gans, 1989; Barton, 1990; Elison, 1995; Long and Soignard, 2016; Howland, 2016; Hyndman, 2017; Long et al., 2018) (e.g., Fig. 4C); (3) modern Great Basin thermal gradients are high (Lachenbruch, 1978; Blackwell et al., 2011); and (4) observations from other contractional orogens and orogenic plateaus suggest elevated thermal gradients, such as in the Himalaya, the Tibetan Plateau, and the Andes (e.g., Francheteau et al., 1984; Derry et al., 2009; Cardoso et al., 2010). High modern thermal gradients do not bear on Mesozoic temperatures, but demonstrate that thermal gradients ≤ 25 °C/km have generally not affected the Great Basin geology since the Mesozoic. The peak temperature vs. stratigraphic depth plot in Fig. 4 (Long and Soignard, 2016; Zuza et al., 2020) reveals high geothermal gradients (≥ 40 °C/km) that do not overlap the predictions for deep Windermere thrust burial (shown in red shading). Although Long and Soignard's (2016) hot geothermal gradient was interpreted to result from a proximal Cretaceous intrusion, their study represents a case study for explaining elevated heatflow across much of eastern Nevada (e.g., Barton, 1990). Throughout Earth's Phanerozoic history, available constraints suggest that hinterland regions commonly have thermal gradients ≥ 30 °C/km (Brown et al., 2020).

Most Carlin-type gold deposits (CTD) in northeast Nevada are thought to have been mineralized at relatively shallow depths (<5 km) (e.g., Kuehn and Rose, 1995; Arehart, 1996; Cline and Hofstra, 2000; Nutt and Hofstra, 2003). Therefore, the simplest case for the Eocene Long Canyon deposit in the Pequop Mountains is that it was mineralized at similarly shallow levels. Given that major extension and exhumation did not initiate until the Oligocene or Miocene (Wright and Snoke, 1993; Colgan and Henry, 2009; Henry et al., 2011), the deep burial model would require Long Canyon to have mineralized at great depths >15 km, which is dissimilar to other CTDs.

Lastly, deep burial models require greater magnitudes of extension to exhume rocks from ~30 km depth. These models favor earlier Cenozoic, or even latest Cretaceous, initiation of exhumation (e.g., McGrew

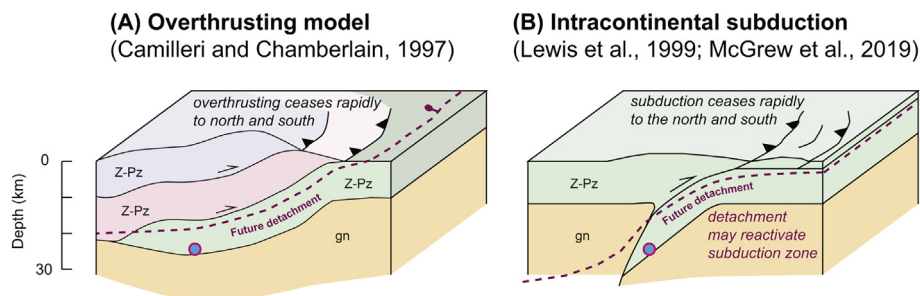
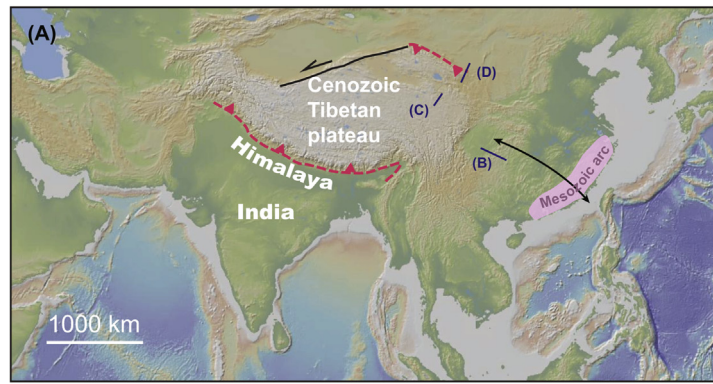
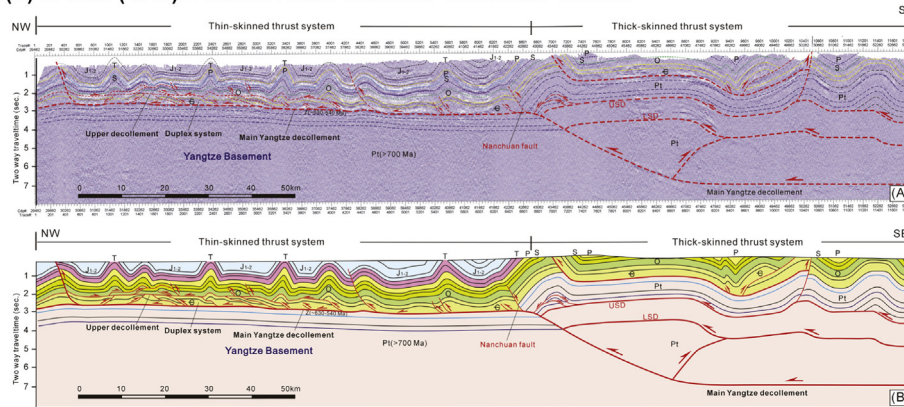


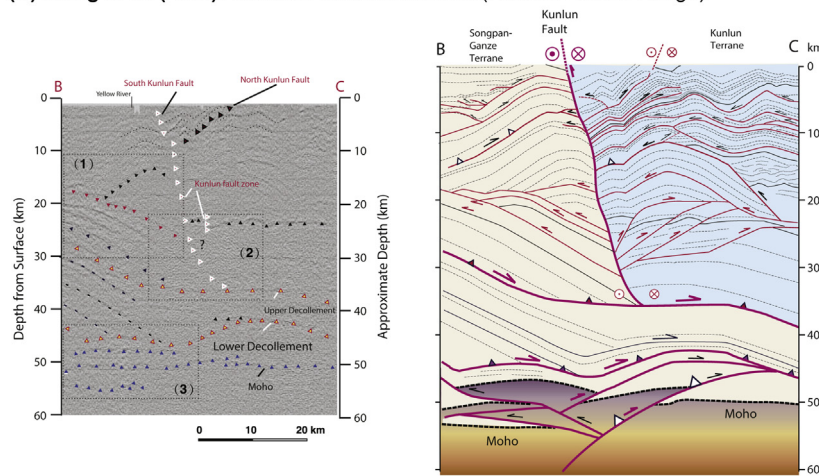
Fig. 7. Block models to explain proposed deep burial in northeast Nevada either via (A) significant overthrusting or (B) intracontinental subduction. Z-Pz: Neoproterozoic–Paleozoic passive margin stratigraphy; gn: schematic representation of Proterozoic basement gneiss.



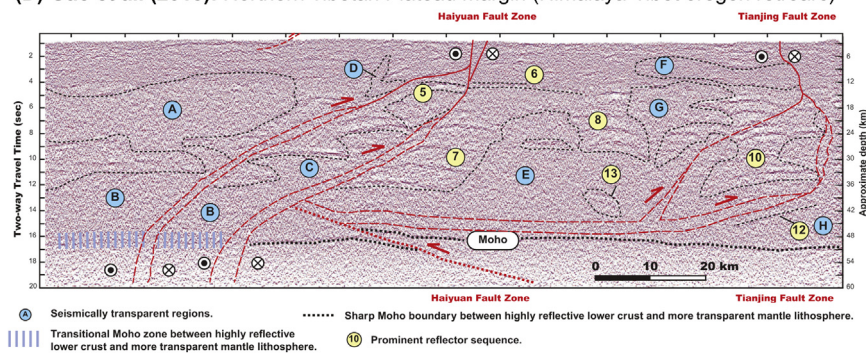
(B) Li et al. (2018): Western Pacific Mesozoic “Cordilleran” retroarc



(C) Wang et al. (2011): Tibetan Plateau hinterland (Eastern Kunlun Range)



(D) Gao et al. (2013): Northern Tibetan Plateau margin (Himalaya-Tibet orogen retroarc)



● Seismically transparent regions. ⋯ Sharp Moho boundary between highly reflective lower crust and more transparent mantle lithosphere.
||||| Transitional Moho zone between highly reflective lower crust and more transparent mantle lithosphere. ● Prominent reflector sequence.

Fig. 8. Compilation of high-resolution deep seismic reflection profiles across major contractional fold-thrust belts in Asia, including the western Pacific retroarc fold-thrust belt (Li et al., 2018), the northern margin of the Tibetan Plateau (Gao et al., 2013), the Himalayan fold-thrust belt (Gao et al., 2016), and the Eastern Kunlun Range in the central Tibetan Plateau (Wang et al., 2011). These observations may serve as analogs for the types of structures observed across a developing orogenic plateau and/or within the retro-arc fold-thrust belt.

and Snee, 1994; Camilleri and Chamberlain 1997; McGrew et al., 2000). Geologic evidence suggests relatively minor extension in the Eocene, during the deposition of the Eocene Elko Formation with relatively minor surface breaking faults (e.g., Lund Snee et al., 2016; Smith et al., 2017). Oligocene basin and fault history are negligible, with the exception of the thin and relatively isolated Clover Creek sequence just east of the East Humboldt Range (e.g., McGrew and Snoke, 2015). Widespread Miocene-to-present basins demonstrably record this phase of deformation. In this respect, non-lithostatic overpressure models that require less burial accordingly require less exhumation, with Neoproterozoic rocks being brought from ≤ 15 km to the surface by the present. Our understanding of Miocene-to-present extension and exhumation is compatible with this kinematic history (Henry, 2008; Colgan and Henry, 2009; Colgan et al., 2010; Henry et al., 2011).

6.3. Further arguments against deep burial

Above we argue that the REWP rocks were not deeply buried, and therefore the published *P-T* datasets do not represent lithostatic depths. In our view, the regional geology is inconsistent with deep burial models. That said, large magnitude shortening has previously been invoked in both the REWP and Snake Range (Camilleri and Chamberlain, 1997; Lewis et al., 1999; McGrew et al., 2019). Here we examine these scenarios and critically evaluate their kinematic predictions for the middle-upper crust.

To bury rocks from a 10–15-km stratigraphic depth to >25 km requires either a 15+ km thick overthrust sheet, or several thrust panels, that buries the passive margin sequence in situ—i.e., in an upper crust reference frame, the rocks are relatively stationary and get buried by thrust panels. This has been proposed for the REWP (e.g., Camilleri and Chamberlain, 1997; Camilleri, 1998) (Fig. 7A). Alternatively, the passive margin sequence is brought down to great depths (25–30 km) along a very steep intracontinental subduction-like megathrust—i.e., in an upper crust reference frame, these rocks are transported to depth (Fig. 7B). Lewis et al. (1999) proposed this for the Snake Range, and a similar model has been envisioned for the REWP (McGrew et al., 2019).

Although the steep intracontinental subduction-like megathrust model is appealing to recreate observed pressure estimates, we argue that it is unrealistic because it (1) is atypical of known thrust systems within orogenic plateaus locally (i.e., the Nevadaplano) and globally, and (2) results in kinematic requirements that are hard to reconcile with geologic observations from northeastern Nevada. The Late Cretaceous REWP was located within the inferred Nevadaplano orogenic plateau. At this longitude, Cretaceous thrust structures are preserved to the south, including the Central Nevada thrust belt and Eureka culmination (Long et al., 2014; Di Fiori et al., 2020) and thrust system in the Confusion Range (Greene, 2014). However, these faults involve relatively low magnitude fault-bend fold thrust-fault geometries that did not significantly bury the footwall rocks. Related to this, regional compilations of erosion levels beneath Cenozoic rocks (i.e., recording Cretaceous erosion and exhumation) show relatively minimal pre-Cenozoic exhumation, primarily focused along the aforementioned structures (Armstrong, 1968; Gans and Miller, 1983; Van Buer et al., 2009; Long, 2012). Therefore, invoking high-magnitude localized intracontinental subduction or megathrusting just near REWP is not justifiable based on the regional deformation pattern.

Examining modern analogs, geophysical and geological investigations around the Tibetan and Andean (Altiplano-Puna) plateaus have generated a wealth of data on the styles of continental deformation within and around orogenic plateaus. For example, SinoProbe seismic reflection profiling, coupled with decades of geologic mapping, have revealed the style of crustal shortening in the active Himalayan-Tibetan orogen and the Mesozoic western Pacific Mesozoic “Cordilleran-style” retro-arc fold-thrust belt (Fig. 8). These profiles image structures from the surface to the Moho (Wang et al., 2011; Dong et al., 2013; Gao et al., 2013; Li et al., 2018; Fig. 8), and none shown the envisioned

intra-continental subduction zone geometries (Fig. 7) that wholesale transport coherent packages of upper crustal rocks to depths as envisioned in the Lewis et al. (1999) model. Similarly, balanced cross sections and structural models of the Andes, which is thought to represent an active contemporary analog to the North American Cordillera, do not document steep localized intra-continental subduction systems that transport upper crustal rocks to depths of 25–30 km (e.g., McQuarrie, 2002; Anderson et al., 2017).

Another complication is that deep-burial models in northeast Nevada require that after high-magnitude contraction-related burial, subsequent extension and plateau collapse exhumed the deeply buried rocks along a detachment fault that is perfectly parallel to the thrust structures (Fig. 7). That is, the exhumation process impeccably removed the overburden rocks and left no record of prior high-magnitude overthrusting and/or intracontinental subduction. Contractional and extensional structures commonly dip or plunge to reveal different structural depths; this is the basis for how orogen-scale cross sections are drafted (e.g., Boyer and Elliot, 1982; Yin, 2006; Webb et al., 2007). Thus, it is perhaps too convenient that the envisioned exhumation of deeply buried rocks in northeast Nevada left to trace prior high-magnitude shortening.

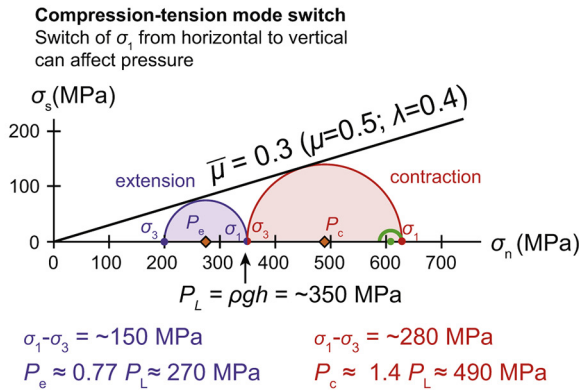
There are also kinematic consequences of bringing upper crust to 25–30 km depths in the Late Cretaceous, because this requires at least 30 km of horizontal shortening in the upper crust to accommodate that vertical displacement (assuming steep 60° fault; more shortening required for a shallower structure). In the simplest case, this shortening occurs on the footwall side of the megathrust, although wedge tectonics can partition some of this deformation on the hanging wall side (Yin, 2006; Zuza et al., 2019b). Upper crustal shortening near and east of the REWP is (1) probably mostly Jurassic in age, and (2) involves slip of <10 km on well documented structures like the Independence thrust (Fig. 2; Camilleri and Chamberlain, 1997; Zuza et al., 2020). Orogen-scale kinematic models of the Sevier fold-thrust belt and its hinterland assume that the REWP was buried deeply in the hinterland region prior to ca. 85 Ma, but these models do not specify what structure was responsible for this burial (e.g., Long and Kohn, 2020).

There are also lateral kinematic problems: 30 km of horizontal transport to subduct/underthrust the upper crust at REWP latitudes, which would have been located somewhere in the central part of the Nevadaplano, should be expressed somehow to the north and south of the REWP. That is, these models imply (1) high magnitude shortening strain to the north and south of the REWP that is not observed, and (2) thickened crust of the Nevadaplano was generated via ~ 30 km intracontinental subduction, which implies that regions outside of the REWP were never thickened because they lack this high magnitude shortening. Most models of the Nevadaplano infer that it was mostly continuous in a north-south direction (e.g., Coney and Harms, 1984; Bahadori et al., 2018), implying that localized high strain shortening or intracontinental subduction in the REWP and northern Snake Range was not a common mechanism for crustal thickening and plateau development. Just south of the high pressure estimates from the East Humboldt Range, the central-southern Ruby Mountains were never deeply buried (Fig. 1) (e.g., Barnes et al., 2001; Colgan et al., 2010).

6.4. Non-lithostatic overpressure and possible explanations

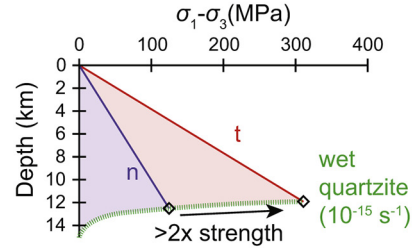
As outlined in this work, there has been rigorous discussion over the past 30+ years about Cordilleran metamorphic core complexes in eastern Nevada, with geobarometry data at odds with palinspastic reconstructions using mapping and field relationships (Miller et al., 1983; Hodges et al., 1992; Lewis et al., 1999; Cooper et al., 2010; Hallett and Spear, 2015). We propose that non-lithostatic pressure may have been significant for the REWP rocks, which simultaneously suggests that the published pressure estimates are accurate and the field relationships are valid. Fig. 5B shows the inferred overpressure ratios (recorded pressures, P , over lithostatic pressures for a sample, P_L), and allowing

(A) P_L set at ~350 MPa based on minor crustal thickening and Hurlow et al. (1991) estimate



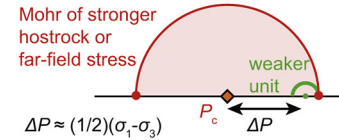
Sibson (1974) and Anderson (1951) fault modes

Thrust-mode rocks are >2x stronger than normal-fault rocks



Viscosity heterogeneity

~10x viscosity contrast can cause pressure perturbation equal to half the rock strength



(B) Hurlow et al. (1991) estimate is P_e implying ~425 MPa represents lithostatic depths

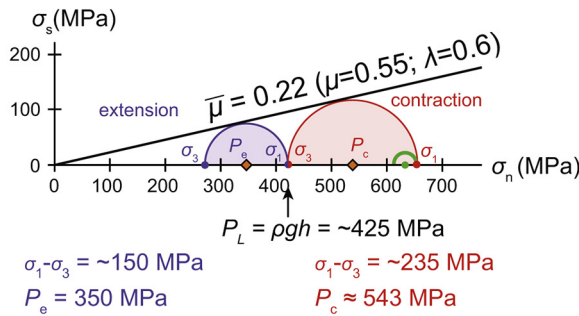


Fig. 9. Example calculations for non-lithostatic overpressure in the Nevadan metamorphic core complexes, using P estimate of Hurlow et al. (1991) because it was obtained from the mylonitic shear zone, yielded pressures that correspond to only slightly deeper than stratigraphic depths, and thus can be a test scenario of possible overpressure. Calculations use a combination of compression-tension mode switching of Yamato and Brun (2017), the Schmid and Podladchikov (2003) model for a weak inclusion with a stronger matrix (e.g., Moulas et al., 2014), and a validation of why rocks under compression (thrust, t) are stronger than under tension (normal fault, n) based on classic Anderson (1905) and Sibson (1974) theory. (A) Lithostatic pressure (P_L) is set to ~350 MPa (~13 km depth); the strength of the rock under Cenozoic extension ($\sigma_3 - \sigma_1$) is given by local piezometer-based estimates (Hacker et al., 1990; Levy and Zuza, 2019) and taken as ~150 MPa; for extension, σ_1 is assumed to be vertical and thus $\sigma_1 = P_L$ and for contraction, σ_3 is assumed vertical and $\sigma_3 = P_L$; for the same rock types, the strength of the rock under contraction is constrained by a yield envelope with no cohesion that envelops the Mohr circle for the rock under extension (i.e., $\bar{\mu} = 0.3$, which is satisfied by $\mu = 0.5$ and $\lambda = 0.4$), which equates to a strength of ~280 MPa; if σ_2 is $\sim(\sigma_1 + \sigma_3)/2$, the predicted pressure during contraction (P_c) could half of strength (~140 MPa) higher than P_L or $\sim 1.4 \times P_L$, which is ~490 MPa; and weaker rocks under the same far-field stress must experience pressures that are significantly higher, as shown with the green Mohr circle that shares the same σ_1 as the red Mohr circle, which could yield pressures ≥ 600 MPa (e.g., Moulas et al., 2014). In this example, tectonic mode switching and strength heterogeneities could result in pressures that would suggest depths of ~23 km. Note that thrust-mode (contractional) rocks are >2x stronger than normal-fault-mode rocks (extensional) based on classic studies (Anderson, 1905; Sibson, 1974). (B) Similar to Fig. 8A, except Hurlow et al. (1991) pressure estimate is taken as pressure under extension (P_e), not P_L , which suggests P_L could be ~425 MPa (~16 km), P_c could be ~543 MPa (~18 km), and peak pressures recorded in the weaker layers could be ~625 MPa (~24 km).

~4 km of structural thickening—which is justifiable based on observed thrust-fault structures—overpressure ratios range from 1 to $2 \times$.

Based on the end-member categories for non-lithostatic overpressure summarized in Fig. 3, general conditions that might favor and enhance overpressure include: (1) regions adjacent to thickened plateaus (Schmalholz et al., 2014), (2) rocks with synkinematic local partial melt generation (Chu et al., 2017), (3) shear zones consisting of rocks with heterogeneous strengths (Schmalholz and Podladchikov, 2013; Marques et al., 2018), and (4) switching tectonic regimes from contraction to extension (Yamato and Brun, 2017). The metamorphic core complexes in eastern Nevada meet all of these conditions based on their geologic/structural setting. As outlined above, the REWP region involved regional contractional deformation in the Late Cretaceous, when peak pressures were recorded, and the region subsequently switched to being under extension during the Cenozoic, during REWP core complex formation and Basin and Range extension. There may

have additionally been shorter timescale switches from contraction to extension during the Late Cretaceous (e.g., Camilleri et al., 1997), including pulses of synconvergent extension as has been argued for in the nearby Raft River-Albion-Grouse Creek metamorphic core complex (e.g., Wells et al., 2012).

The following discussion uses observations from the East Humboldt Range to explain higher pressure estimates of ~7 kbar from rocks that may not be buried deeper than ~15 km, or ~4 kbar of lithostatic pressure. These arguments stem from the above groups of overpressure models (Fig. 3). We start by assuming Hurlow et al. (1991)'s pressure estimate from the Neoproterozoic McCoy Creek Group of ~3.5 kbar accurately reflects lithostatic conditions (~13 km). We also assume that the average rock type in this region has a strength (differential stress) of 150 MPa in the extensional regime, which is based on our own calcite and quartz paleopiezometric calculations (Levy and Zuza, 2019), and data from the Whipple detachment in California, which has a peak

Table 2
Predictions of overpressure versus lithostatic pressure estimates for REWP geobarometric data.

Predictions												
		Burial mechanism	Map relationships	Deep burial extent relative to other Cordillera hinterland structures	Predicted geothermal gradient (Γ)	Voluminous intrusions vs thermal structure	Crustal melt generation	Relationships between melt generation and deformation	Relationships of REWP peraluminous granite to "Cordilleran two-mica belt"	Post-plateau extension magnitude	Timing of earliest extension	Depth of Eocene Long Canyon gold mineralization
Model for pressure estimates	Record deep burial depths	Overthrusting or intracontinental subduction/ underthrusting to depths 2–3 × stratigraphic depths	Structural juxtaposition of lower stratigraphy over upper stratigraphy; or complete obscuration by later extension	Spatially restricted, possibly in zones of melts and thermal weakening; atypical of other Cordilleran structures	Moderate-to-low (≤ 25 °C/km)	Intrusions post-date high P - T or are too minor to affect recorded Γ	Thickening required to bring local McCoy Creek pelites to $T \geq 700$ °C with low Γ	Thickening and prograde P - T path predates peraluminous melt generation	Disconnected – required deep localized burial atypical along strike	High enough to exhume rocks from 30 km	Late Cretaceous–early Cenozoic	>10–15 km, dissimilar to Carlin-type gold deposits to the west
	Reflect non-lithostatic pressure without deep burial	Moderate-to-low magnitude crustal shortening buries stratigraphy several kilometers	Kilometer-scale thrust juxtapositions and duplications	Similar to other structures along strike, possible enhanced deformation due to localized intrusions and thermal weakening	Moderate-to-high (30–40+ °C/km)	Intrusions drive high Γ	Westward basement underthrusting generated anatectic melts, raised Γ , and allowed further melting of pelites at near stratigraphic depths	Melt generation due to underthrust sediments from east; heat from intrusions drives more melting and ductile contractional deformation (e.g., nappe structures)	Genetically related to others in the two-mica belt, potentially due to westward underthrusting of pelitic rocks	Moderate to exhume rocks from ≤ 15 km.	Oligocene–Miocene	≤ 3 –5 km, similar to Carlin-type gold deposits to the west

* Two-mica belt of Miller and Bradfish (1980) stretching from Arizona to Canada.

strength of ~157 MPa (Behr and Platt, 2011; Axen, 2020). These differential stress estimates for the bulk rock are likely minimum estimates, due to effects of thermal softening in the weakened shear zones, such as those modeled numerically by Jaquet and Schmalholz (2018). Because the rocks were most recently under extension, σ_1 is assumed to be subvertical, and here assumed to equal lithostatic pressure, P_L (i.e., 350 MPa). Therefore, the Mohr circle for extension (purple in Fig. 9) extends from 350 MPa (σ_1) to 200 MPa (σ_3). During Mesozoic contraction, σ_3 was subvertical. Assuming some reasonable yield envelope that encompasses both Mohr circles, with effective friction $\bar{\mu}$ of 0.3, a Mohr circle can be drawn for the contractional domain (e.g., Yamato and Brun, 2017). This Mohr circle implies a differential strength during contractional deformation of ~280 MPa, which suggests that σ_1 was >600 MPa.

The classic Anderson (1905) and Sibson (1974) fault models suggest that a column of thrust-mode rocks are twice as strong as normal-fault-mode rocks, which is compatible with our claim that the ~150 MPa strength of normal-fault rocks is half that of thrust-mode rock strength (Fig. 9A). Critical wedge theory is also consistent with this assertion (e.g., Dahlen, 1990; Moulas et al., 2019). There is negligible piezometer-based documentation of stronger thrust-mode shear zones, although Kidder et al. (2012) presented differential stresses approaching ~200 MPa for Taiwan thrust faults. Piezometric determination of higher stresses may be difficult given that it implies dynamically recrystallized grain sizes <3 μm , which would be hard to resolve optically due to thin-section-thickness limitations and thus may benefit from targeted scanning electron microscope (SEM) imaging. Furthermore, post-kinematic annealing (e.g., Hacker et al., 1992) or departures from steady-state assumptions (Soleymani et al., 2020) can increase grain size, leading to apparently lower stress estimates.

Depending on the relative magnitude of σ_2 , the mean stress (pressure) during compression/contraction, P_c , is around 5 kbar, or 1.4 \times the starting lithostatic pressure (Fig. 9A). Lastly, heterogeneous rock strength, as observed in northeast Nevada with limestone marbles and pelites flowing around stronger dolomite and quartzite, can enhance this pressure difference. Tying the Mohr circles to σ_1 , weaker rocks have a smaller Mohr diameter and thus their implied mean stress will shift higher (Moulas et al., 2014; Fig. 9A). Other studies have shown the mean stress of these weaker phases may approach the σ_1 in Fig. 9A (e.g., Moulas et al., 2014, 2019). In this example, this could yield ~6 kbar pressures, or 1.6 \times the starting lithostatic pressure (Fig. 9A).

Alternatively, we can start with the assumption that the Hurlow et al. (1991) observation of ~350 MPa is actually the mean stress under extension, P_e , and thus σ_1 , which equals P_L , was ~425 MPa (Fig. 9B). Again using a common yield envelope, a contractional Mohr circle is drawn to the right at higher normal stress values, which results in a differential stress of ~235 MPa (Fig. 9B). The mean stress of this circle would be around ~550 MPa, and heterogeneous rock rheology could result in local pressure estimates near ~650 MPa (Fig. 9B), which would be 1.3–1.5 \times the starting lithostatic pressure (Fig. 9B).

The autoclave effect (Vrijmoed et al., 2009; Chu et al., 2017; Cutts et al., 2020) could drive these pressures higher. Namely, the REWP is pervasively intruded by Late Cretaceous leucogranites and Cenozoic sills. Much of the East Humboldt Range and Ruby Mountains classically consists of >2/3 intrusions by volume (e.g., Lee et al., 2003; Howard et al., 2011). Through thermodynamic modeling, Hallett and Spear (2014, 2015) demonstrated that Late Cretaceous leucogranites in the East Humboldt Range were derived from in-situ partial melting of the host rocks, driven by muscovite dehydration reactions. If the surrounding host rocks acted as an encompassing pressure vessel (e.g., Vrijmoed et al., 2009; Gerya, 2015), the lower density of the partial melting and dehydrating mica breakdown may have locally driven overpressure. This effect does not require perfectly rigid or infinitely strong bounding wallrock, as long as the timescales of pressure buildup are faster than

viscous relaxation (e.g., Zhong et al., 2018). Chu et al. (2017)'s interpretation of the autoclave effect was partially based on observations of short timescales of high-pressure metamorphism. To this end, Hoiland et al. (2019) showed titanium diffusion profiles for quartz included in garnet in the northern Snake Range that implied metamorphism timescales that were shorter (~ 1 Myr) than expected for regional Barrovian or burial metamorphism (~10 Myr). These short timescales of metamorphism may be a diagnostic feature of non-lithostatic overpressure, and would produce pressure perturbations at rates much faster than viscous relaxation.

Pressure estimates in the REWP vary spatially, but with no systematic decrease in pressure with elevation or longitude, as might be expected if the variations were due to differential burial. For example, McGrew et al. (2000)'s pressure estimates span ~5.5 kbar to 10.7 kbar, but there is no correlation of these pressures with elevation (range from ~2.5 km to ~3.2 km) or mapview location. That said, typical uncertainties for pressure estimates are ~1 kbar (2.6 km lithostatic pressure), so spatial burial variations would not be resolvable at scales finer than ~5 km. However, the lack of any spatial trend suggests that the pressure variations may be due to other variables, such as rock strength heterogeneities or autoclave-related intrusion density. A future test of these non-lithostatic pressure variations might involve careful documentation of pressure estimates with respect to these variables (e.g., intrusion density, lithology).

As a final consideration, this region and the northern Snake Range were located along the eastern margin of the growing Nevadaplano orogenic plateau in the Late Cretaceous (Fig. 1A; e.g., DeCelles, 2004) when peak pressures were recorded. Schmalholz et al. (2014) demonstrated via 2D numerical models that significant deviatoric stresses can arise from gravitational potential energy (GPE) variations in an orogen, regardless of rock strength and viscosity considerations discussed above. Their model considered a plateau adjacent to lower topography using a thin-viscous sheet approximation (i.e., vertically averaged stress with homogenous viscosity), and generated vertically averaged overpressure of up to 60 MPa in the lowlands. Incorporating vertical variations in material properties would tend to focus and increase overpressure in some rocks while it decreases in others to vertically average at ~60 MPa. 3D modeling by Lechmann et al. (2014) of the Himalayan-Tibetan orogen showed tectonic overpressure of 500–800 MPa for the crust adjacent to the growing Tibetan Plateau and for underthrust portions of the Indian indenter. The spatial relation of Cordillera metamorphic core complexes that possibly record non-lithostatic overpressure and the edge of the growing Nevadaplano orogenic plateau suggests that GPE differences may contribute to overpressure, as argued by Lechmann et al. (2014) and Schmalholz et al. (2014).

7. Conclusions

Non-lithostatic overpressure is a controversial topic in the Earth Sciences. Theory and modeling suggest that rocks may experience non-lithostatic pressure conditions, but confirmed geological observations of this phenomena are sparse. Here we suggest that the long-standing debate regarding North America Cordilleran metamorphic core complexes, and the depth of rocks that they exhume, may reflect non-lithostatic overpressure. In particular, the well-documented ~12–15 km thick Neoproterozoic–Paleozoic passive margin strata of western North America provide a reliable structural marker for restorations of burial depth. Published geobarometry from both the northern Snake Range and Ruby Mountains–East Humboldt Range–Wood Hills–Pequop Mountains (REWP) metamorphic core complexes suggests that these strata were buried to depths ≥ 20 –25 km, but palinspastic reconstructions based on detailed geologic mapping suggests that they were not buried significantly deeper than their stratigraphic depths. Here we focused on the REWP region, and outlined model predictions

for and against deep burial models to test these competing hypotheses. Most geologic evidence does not favor deep burial, which implies tectonic overpressure may cause non-lithostatic pressure conditions for the REWP rocks. The exact mechanism for non-lithostatic overpressure remains unconstrained. Most published models for non-lithostatic pressures may apply in the REWP based on the regional geologic history, including impacts from deviatoric/differential stress considerations, tectonic mode switching, and the autoclave effect driven by dehydration melting.

Declaration of Competing Interest

The authors declare that they have no known competing financial interests or personal relationships that could have appeared to influence the work reported in this paper.

Acknowledgments

This research was supported by USGS STATEMAP (G16AC00186, G17AC00212, G18AC00198, G19AC00383), the Tectonics program of the National Science Foundation (EAR 1830139), and startup funds at UNR. We appreciate constructive comments and feedback from reviewers Jay Chapman, Dave Pattinson, and Evangelos Moulas, and handling by Associate Editor Richard Palin. Chuck Thorman and Art Snoke are thanked for great discussions in the field that helped us learn the geology of northeast Nevada and pointed to some of the outstanding issues. Our work with Chris Henry, Seth Dee, and Sean Long have guided aspects of this research. This manuscript also benefited from encouragement during the virtual European Geophysical Union conference. The views and conclusions contained in this document are those of the authors and should not be interpreted as necessarily representing the official policies, either expressed or implied, of the U.S. Government. Any use of trade, firm, or product names is for descriptive purposes only and does not imply endorsement by the U.S. Government.

Appendix A. Supplementary data

Supplementary data to this article can be found online at <https://doi.org/10.1016/j.gsf.2020.10.006>.

References

- Latham, 2016. Mechanisms and patterns of strain related to late Mesozoic tectonic shortening on the Independence Thrust, Pequoop Mountains, Elko County Nevada. Keck Geology Consortium Short Contributions 29.
- Thorman, C.H., 1962. Structure and stratigraphy of the Wood Hills and a portion of the northern Pequoop Mountains, Elko County, Nevada. PhD thesis. University of Washington, Seattle, p. 218.
- Allmendinger, R.W., 1992. Thrust and fold tectonics of the western United States exclusive of the accreted terranes. In: Burchfiel, B.C., Lipman, P., Zoback, M.L. (Eds.), *The Cordilleran orogen: Conterminous U.S. Geological Society of America, Geology of North America*, Boulder, Colorado, pp. 583–607.
- Allmendinger, R.W., Miller, D.M., Jordan, T.E., 1984. Known and inferred Mesozoic deformation in the hinterland of the Sevier belt, Northwest Utah. In: Kerns, G.J., Kerns, R.L. (Eds.), *Geology of Northwest Utah*. Utah Geological Association Publication, Southern Idaho and Northeast Nevada, pp. 21–34.
- Anderson, E.M., 1905. The dynamics of faulting. *Trans. Edinb. Geol. Soc.* 8, 387–402.
- Anderson, R.B., Long, S.P., Horton, B.K., Calle, A.Z., Ramirez, V., 2017. Shortening and structural architecture of the Andean fold-thrust belt of southern Bolivia (21°S): implications for kinematic development and crustal thickening of the central Andes. *Geosphere* 13, 538–558.
- Angel, R.J., Mazzucchelli, M.L., Alvaro, M., Nimis, P., Nestola, F., 2014. Geobarometry from host-inclusion systems: the role of elastic relaxation. *Am. Mineral.* 99, 2146–2149.
- Angel, R.J., Mazzucchelli, M.L., Alvaro, M., Nestola, F., 2017. EosFit-Pinc: a simple GUI for host-inclusion elastic thermobarometry. *Am. Mineral.* 102, 1957–1960.
- Angel, R.J., Murri, M., Mihailova, B., Alvaro, M., 2019. Stress, strain and Raman shifts. *Zeitschrift für Kristallographie-Crystal. Mater.* 234, 129–140.
- Arehart, G.B., 1996. Characteristics and origin of sediment-hosted disseminated gold deposits: a review. *Ore Geol. Rev.* 11, 383–403.
- Armstrong, R.L., 1968. Sevier orogenic belt in Nevada and Utah. *Geol. Soc. Am. Bull.* 79, 429–458.
- Armstrong, R.L., Hansen, E., 1966. Cordilleran infrastructure in the eastern Great Basin. *Am. J. Sci.* 264, 112–127.
- Axen, G.J., 2020. How a strong low-angle normal fault formed: the Whipple detachment, southeastern California. *Geol. Soc. Am. Bull.* 132 (9–10), 1817–1828.
- Bachl, C.A., Miller, C.F., Miller, J.S., Faulds, J.E., 2001. Construction of a pluton: evidence from an exposed cross section of the Searchlight pluton, Eldorado Mountains, Nevada. *Geol. Soc. Am. Bull.* 113 (9), 1213–1228.
- Bahadori, A., Holt, W.E., Rasbury, E.T., 2018. Reconstruction modeling of crustal thickness and paleotopography of western North America since 36 Ma. *Geosphere* 14, 1207–1231.
- Barnes, C.G., Burton, B.R., Burling, T.C., Wright, J.E., Karlsson, H.R., 2001. Petrology and geochemistry of the late Eocene Harrison Pass pluton, Ruby Mountains core complex, northeastern Nevada. *J. Petrol.* 42, 901–929.
- Barton, M.D., 1990. Cretaceous magmatism, metamorphism, and metallogeny in the east-central Great Basin. In: Anderson, J.L. (Ed.), *The Nature and Origin of Cordilleran Magmatism*. Geological Society of America Memoir 174, pp. 283–302.
- Bedell, R., Struhsacker, E., Craig, L., Miller, M., Coolbaugh, M., Smith, J., Parratt, R., 2010. The Pequoop mining district, Elko County, Nevada: An evolving new gold district. In: Goldfarb, R.J., Marsh, E.E., Monecke, T. (Eds.), *The Challenge of Finding New Mineral Resources: Global Metallogeny, Innovative Exploration, and New Discoveries*. Society of Economic Geologists, pp. 29–56.
- Behr, W.M., Platt, J.P., 2011. A naturally constrained stress profile through the middle crust in an extensional terrane. *Earth Planet. Sci. Lett.* 303, 181–192.
- Berman, R.G., 1991. Thermobarometry using multi-equilibrium calculations; a new technique, with petrological applications. *Can. Mineral.* 29, 833–855.
- Blackwell, D., Richards, M., Frone, Z., Batir, J., Ruzo, A., Dingwall, R., Williams, M., 2011. Temperature at depth maps for the conterminous US and geothermal resource estimates. *Geotherm. Resour. Council Trans.* 35 (2), 1545–1550.
- Bohlen, S.R., Wall, V.J., Boettcher, A.L., 1983. Experimental investigations and geological applications of equilibria in the system FeO-TiO₂-Al₂O₃-SiO₂-H₂O. *Am. Mineral.* 68, 1049–1058.
- Bonazzi, M., Tumiati, S., Thomas, J.B., Angel, R.J., Alvaro, M., 2019. Assessment of the reliability of elastic geobarometry with quartz inclusions. *Lithos* 350–351, 105201.
- Boyer, S.E., Elliott, D., 1982. Thrust systems. *AAPG Bull.* 66, 1196–1230.
- Brown, T.H., Berman, R.G., Perkins, E.H., 1988. GeO-Calc: Software package for calculation and display of pressure-temperature-composition phase diagrams using an IBM or compatible Personal Computer. *Comput. Geosci.* 14, 279–289.
- Brown, M., Johnson, T., Gardiner, N.J., 2020. Plate tectonics and the archaic earth. *Annu. Rev. Earth Planet. Sci.* 48 (1). <https://doi.org/10.1146/annurev-earth-081619-052705>.
- Burchfiel, B.C., Davis, G.A., 1975. Nature and controls of Cordilleran orogenesis, western United States-Extension of an earlier synthesis. *Am. J. Sci.* 275A, 363–396.
- Burchfiel, B.C., Cowan, D.S., Davis, G.A., 1992. Tectonic overview of the Cordilleran orogen in the western United States. In: Burchfiel, B.C., Lipman, P.W., Zoback, M.L. (Eds.), *Geology of North America, The Cordilleran orogen: Conterminous U.S. Geological Society of America*, Boulder, Colorado, G-3.
- Camilleri, P.A., 1998. Prograde metamorphism, strain evolution, and collapse of footwalls of thick thrust sheets: a case study from the Mesozoic Sevier hinterland USA. *J. Struct. Geol.* 20, 1023–1042.
- Camilleri, P., 2010. Geologic map of the northern Pequoop Mountains, Elko County, Nevada. Nevada Bureau of Mines and Geology Map 171.
- Camilleri, P.A., Chamberlain, K.R., 1997. Mesozoic tectonics and metamorphism in the Pequoop Mountains and Wood Hills region, northeast Nevada: Implications for the architecture and evolution of the Sevier orogen. *Geol. Soc. Am. Bull.* 109, 74–94.
- Camilleri, P., Yonkee, A., Coogan, J., DeCelles, P., McGrew, A., Wells, M., 1997. Hinterland to foreland transect through the Sevier Orogen, northeast Nevada to north central Utah: Structural style, metamorphism, and kinematic history of a large contractional orogenic wedge. *Brigham Young Univ. Geol. Stud.* 42, 297–309.
- Cao, W., Yang, J., Zuza, A.V., Ji, W.Q., Ma, X.X., Chu, X., Burgess, Q.P., 2020. Crustal tilting and differential exhumation of Gangdese Batholith in southern Tibet revealed by bedrock pressures. *Earth Planet. Sci. Lett.* 543, 116347.
- Cardoso, R.R., Hamza, V.M., Alfaro, C., 2010. Geothermal resource base for South America: A continental perspective. *Proceedings World Geothermal Congress 2010*, Bali, Indonesia, 25–29 April 2010.
- Cassel, E.J., Breecker, D.O., Henry, C.D., Larson, T.E., Stockli, D.F., 2014. Profile of a paleo-orogen: High topography across the present-day Basin and Range from 40 to 23 Ma. *Geology* 42, 1007–1010.
- Chapman, J.B., Ducea, M.N., DeCelles, P.G., Profeta, L., 2015. Tracking changes in crustal thickness during orogenic evolution with Sr/Y: an example from the north American Cordillera. *Geology* 43, 919–922.
- Chu, X., Ague, J.J., Podladchikov, Y.Y., Tian, M., 2017. Ultrafast eclogite formation via melting-induced overpressure. *Earth Planet. Sci. Lett.* 479, 1–17.
- Cline, J.S., Hofstra, A.A., 2000. Ore-fluid evolution at the Getchell Carlin-type gold deposit, Nevada, USA. *Eur. J. Mineral.* 12, 195–212.
- Coats, R.R., 1987. *Geology of Elko County, Nevada*. Nevada Bureau of Mines and Geology Bulletin 101.
- Colgan, J.P., Henry, C.D., 2009. Rapid middle Miocene collapse of the Mesozoic orogenic plateau in north-central Nevada. *Int. Geol. Rev.* 51, 920–961.
- Colgan, J.P., Howard, K.A., Fleck, R.J., Wooden, J.L., 2010. Rapid middle Miocene extension and unroofing of the southern Ruby Mountains, Nevada. *Tectonics* 29 (6), TC6022.
- Coney, P.J., Harms, T.A., 1984. Cordilleran metamorphic core complexes: Cenozoic extensional relics of Mesozoic compression. *Geology* 12, 550–554.
- Cooper, F.J., Platt, J.P., Anczkiewicz, R., Whitehouse, M.J., 2010. Footwall dip of a core complex detachment fault: Thermobarometric constraints from the northern Snake Range (Basin and Range, USA). *J. Metamorph. Geol.* 28, 997–1020.
- Crafton, A.E.J., 2007. *Geologic map of Nevada*. U.S. Geological Survey Data Series 249, 1 CD-ROM.

- Cutts, J.A., Smit, M.A., Vrijmoed, J.C., 2020. Evidence for non-lithostatic pressure in subducted continental crust. *Contrib. Mineral. Petrol.* 175 (1), 3.
- Dahlen, F.A., 1990. Critical taper model of fold-and-thrust belts and accretionary wedges. *Annu. Rev. Earth Planet. Sci.* 18 (1), 55–99.
- DeCelles, P.G., 2004. Late Jurassic to Eocene evolution of the Cordilleran thrust belt and foreland basin system, western USA. *Am. J. Sci.* 304, 105–168.
- DeCelles, P.G., Coogan, J.C., 2006. Regional structure and kinematic history of the Sevier fold-and-thrust belt, central Utah. *Geol. Soc. Am. Bull.* 118, 841–864.
- Dee, S., Henry, C.D., Ressel, M.W., Zuza, A.V., 2017. Preliminary Geologic Map of the North Half of the Independence Valley NW Quadrangle and the Adjacent Part of the Independence Valley NE Quadrangle, Elko County, Nevada, Nevada Bureau of Mines and Geology Open-File Report.
- Derry, L.A., Evans, M.J., Darling, R., France-Lanord, C., 2009. Hydrothermal heat flow near the Main Central thrust, central Nepal Himalaya. *Earth Planet. Sci. Lett.* 286, 101–109.
- Di Fiori, R.V., Long, S.P., Fetrow, A.C., Snell, K.E., Bonde, J.W., Vervoort, J., 2020. Syncontractional deposition of the cretaceous Newark Canyon Formation, Diamond Mountains, Nevada: Implications for strain partitioning within the US Cordillera. *Geosphere* 16 (2), 546–566. <https://doi.org/10.1130/GES02168.1>.
- Dickinson, W.R., 2004. Evolution of the north American cordillera. *Annu. Rev. Earth Planet. Sci.* 32, 13–45.
- Dong, S.W., Li, T.D., Lü, Q.T., Gao, R., Yang, J.S., Chen, X.H., Wei, W., Zhou, Q., 2013. Progress in deep lithospheric exploration of the continental China: a review of the SinoProbe. *Tectonophysics* 606, 1–13.
- Elison, M.W., 1995. Causes and consequences of Jurassic magmatism in the northern Great Basin: Implications for tectonic development. In: Miller, D.M., Busby, C. (Eds.), *Jurassic Magmatism and Tectonics of the North American Cordillera*. Geological Society of America Special Paper 229, pp. 249–265.
- Ferry, J.T., Spear, F.S., 1978. Experimental calibration of the partitioning of Fe and Mg between biotite and garnet. *Contrib. Mineral. Petrol.* 66, 113–117.
- Fletcher, R.C., 2015. Dramatic effects of stress on metamorphic reactions: COMMENT. *Geology* 43, 372.
- Francheteau, J., Jaupart, C., Shen, X.J., Kang, W., Lee, D., Bai, J., Wei, H., Deng, H., 1984. High heat flow in southern Tibet. *Nature* 307, 32–36.
- Gans, P.B., 2000. The northern White Pine Range, in Gans, P.B., and Seedorf, E., eds., *Geology and Ore Deposits 2000*, Field Trip 11, Geological Society of Nevada, p. 83–95.
- Gans, P.B., and Miller, E. L., 1983. Style of mid-Tertiary extension in east-Central Nevada. In: Nash, W.P., Gurgel, K.D. (Eds.), *Geological Excursions in the Overthrust Belt and Metamorphic Complexes of the Intermontane Region*. Utah Geological and Mineral Survey Special Study 59, pp. 107–160.
- Gans, P.B., Miller, E.L., 1983. Style of mid-Tertiary extension in east-central Nevada. Geological excursions in the overthrust belt and metamorphic core complexes of the Intermontane region: Utah Geological and Mineral Survey Special Studies 59 pp. 107–139.
- Gao, R., Wang, H., Yin, A., Dong, S., Kuang, Z., Zuza, A.V., Li, W., Xiong, X., 2013. Tectonic development of the northeastern Tibetan Plateau as constrained by high-resolution deep seismic-reflection data. *Lithosphere* 5, 555–574.
- Gao, R., Lu, Z., Klemperer, S.L., Wang, H., Dong, S., Li, W., Li, H., 2016. Crustal-scale duplexing beneath the Yarlung Zangbo suture in the western Himalaya. *Nat. Geosci.* 9, 555–560.
- Gerya, T., 2015. Tectonic overpressure and underpressure in lithospheric tectonics and metamorphism. *J. Metamorph. Geol.* 33, 785–800.
- Ghent, E.D., Stout, M.Z., 1981. Geobarometry and geothermometry of plagioclase-biotite-garnet-muscovite assemblages. *Contrib. Mineral. Petrol.* 76, 92–97.
- Ghent, E.D., Nicholls, J., Simony, P.S., Sevigny, J.H., Stout, M.Z., 1991. Hornblende geobarometry of the Nelson Batholith, southeastern British Columbia: tectonic implications. *Can. J. Earth Sci.* 28, 1982–1991.
- Greene, D.C., 2014. The confusion Range, west-Central Utah: Fold-thrust deformation and a western Utah thrust belt in the Sevier hinterland. *Geosphere* 10, 148–169.
- Groppo, C., Rolfo, F., Indares, A., 2012. Partial melting in the higher Himalayan Crystallines of Eastern Nepal: the effect of decompression and implications for the 'Channel Flow' model. *J. Petrol.* 53, 1057–1088.
- Hacker, B.R., Yin, A., Christie, J.M., Snoke, A.W., 1990. Differential stress, strain rate, and temperatures of mylonitization in the Ruby Mountains, Nevada: implications for the rate and duration of uplift. *J. Geophys. Res. Solid Earth* 95, 8569–8580.
- Hacker, B.R., Yin, A., Christie, J.M., Davis, G.A., 1992. Stress magnitude, strain rate, and rheology of extended middle continental crust inferred from quartz grain sizes in the Whipple Mountains, California. *Tectonics* 11, 36–46.
- Hallett, B.W., Spear, F.S., 2014. The P-T history of anatectic pelites of the Northern East Humboldt Range, Nevada. Evidence for tectonic loading, decompression, and anatexis. *J. Petrol.* 55, 3–36.
- Hallett, B.W., Spear, F.S., 2015. Monazite, zircon, and garnet growth in migmatitic pelites as a record of metamorphism and partial melting in the East Humboldt Range, Nevada. *Am. Mineral.* 100, 951–972.
- Harrison, T.M., Wielicki, M.M., 2016. From the Hadean to the Himalaya: 4.4 Ga of felsic terrestrial magmatism. *Am. Mineral.* 101, 1348–1359.
- Henry, C.D., 2008. Ash-flow tuffs and paleovalleys in northeastern Nevada: Implications for Eocene paleogeography and extension in the Sevier hinterland, northern Great Basin. *Geosphere* 4, 1–35.
- Henry, C.D., Thorman, C.H., 2015. Preliminary geologic map of the Pequo Summit quadrangle, Elko County, Nevada. Nevada Bureau of Mines and Geology Open File Report 15, p. 8.
- Henry, C.D., McGrew, A.J., Colgan, J.P., Snoke, A.W., Brueseke, M.E., 2011. Timing, distribution, amount, and style of Cenozoic extension in the northern Great Basin. In: Lee, J., Evans, J.P. (Eds.), *Geologic Field Trips to the Basin and Range, Rocky Mountains, Snake River Plain, and Terranes of the U.S. Cordillera*. Geological Society of America Field Guide 21, pp. 27–66.
- Hirth, G., Tullis, J., 1994. The brittle-plastic transition in experimentally deformed quartz aggregates. *J. Geophys. Res. Solid Earth* 99 (B6), 11731–11747.
- Hobbs, B., Ord, A., 2015. Dramatic effects of stress on metamorphic reactions: comment. *Geology* 43, e372.
- Hodges, K.V., Crowley, P.T., 1985. Error estimation and empirical geothermobarometry for pelitic systems. *Am. Mineral.* 70, 702–709.
- Hodges, K.V., Spear, F.S., 1982. Geothermometry, geobarometry and the Al₂SiO₅ triple point at Mt. Moosilauke, New Hampshire. *Am. Mineral.* 67, 1118–1134.
- Hodges, K.V., Snoko, A.W., Hurlow, H.A., 1992. Thermal evolution of a portion of the Sevier hinterland: the northern Ruby Mountains-East Humboldt Range and Wood Hills, northeastern Nevada. *Tectonics* 11, 154–164.
- Hoiland, C.W., Miller, E.L., Coble, M.A., Hourigan, J., Grove, M., 2019. Possible evidence for large departures from lithostatic pressure during Cretaceous metamorphism in the northern Snake Range metamorphic core complex (MCC), Nevada. *Geological Society of America Abstracts with Programs*, p. 51.
- Hose, R.K., Blake Jr., M.C., 1976. *Geology and Mineral Resources of White Pine County*. University of Nevada, Reno, NV, Nevada, p. 113.
- Howard, K.A., 2000. *Geology of the Lamoille Quadrangle, Elko County, Nevada: Nevada Bureau of Mines and Geology Map 125, scale 1:24,000*, p. 4.
- Howard, K.A., Wooden, J.L., Barnes, C.G., Premo, W.R., Snoko, A.W., Lee, S.Y., 2011. Episodic growth of a late cretaceous and Paleogene intrusive complex of pegmatitic leucogranite, Ruby Mountains core complex, Nevada, USA. *Geosphere* 7, 1220–1248.
- Howland, C., 2016. High Thermal Gradient in the Upper Plate of a Core Complex, Determined by Calcite-Dolomite and RSCM Thermometry, Pequo Mountains, NV. BS Honors Thesis, Union College.
- Hudec, M.R., 1992. Mesozoic structural and metamorphic history of the central Ruby Mountains metamorphic core complex, Nevada. *Geol. Soc. Am. Bull.* 104, 1086–1100.
- Humphrey, F.L.S., 1960. *Geology of the White Pine mining district, White Pine County, Nevada*. Nevada Bureau of Mines and Geology Bulletin 57, p. 134.
- Hurlow, H.A., Snoko, A.W., Hodges, K.V., 1991. Temperature and pressure of mylonitization in a Tertiary extensional shear zone, Ruby Mountains-East Humboldt Range, Nevada: Tectonic implications. *Geology* 19, 82–86.
- Hyndman, R.D., 2017. Lower-crustal flow and detachment in the north American Cordillera: a consequence of Cordillera-wide high temperatures. *Geophys. J. Int.* 209, 1779–1799.
- Jaquet, Y., Schmalholz, S.M., 2018. Spontaneous ductile crustal shear zone formation by thermal softening and related stress, temperature and strain rate evolution. *Tectonophysics* 746, 384–397.
- Johnson, M.C., Rutherford, M.J., 1989. Experimental calibration of the aluminum-in-hornblende geobarometer with application to Long Valley caldera (California) volcanic rocks. *Geology* 17, 837–841.
- Jones III, J.V., 1999. *Deformational, Magmatic, and Metamorphic History of the Central Ruby Mountains, Elko County, Nevada*. MS thesis. University of Wyoming, Laramie.
- Jones, C.H., Mahan, K.H., Butcher, L.A., Levandowski, W.B., Farmer, G.L., 2015. Continental uplift through crustal hydration. *Geology* 43, 355–358.
- Ketner, K.B., Day, W.C., Elrick, M., Vaag, M.K., Zimmerman, R.A., Snee, L.W., Saltus, R.W., Wardlaw, B.R., Taylor, M.E., Harris, A.G., 1998. An outline of tectonic, igneous, and metamorphic events in the Goshute-Toano range between Silver Zone pass and White Horse pass, Elko county, Nevada: a history of superposed contractional and extensional deformation. *US Geological Survey* 1593, p. 12.
- Kidder, S., Avouac, J.P., Chan, Y.C., 2012. Constraints from rocks in the Taiwan orogen on crustal stress levels and rheology. *J. Geophys. Res. Solid Earth* 117 (9), B09408.
- Kohn, M.J., 2014. "Thermobarometry": Calibration of spectroscopic barometers and thermometers for mineral inclusions. *Earth Planet. Sci. Lett.* 388, 187–196.
- Kuehn, C.A., Rose, A.W., 1995. Carlin gold deposits, Nevada: origin in a deep zone of mixing between normally pressured and overpressured fluids. *Econ. Geol.* 90, 17–36.
- Lachenbruch, A.H., 1978. Heat flow in the Basin and Range province and thermal effects of tectonic extension. *Pure Appl. Geophys.* 117, 34–50.
- Lechmann, S.M., Schmalholz, S.M., Hetényi, G., May, D.A., Kaus, B.J.P., 2014. Quantifying the impact of mechanical layering and underthrusting on the dynamics of the modern India-Asia collisional system with 3-D numerical models. *J. Geophys. Res. Solid Earth* 119, 616–644.
- Lee, S.Y., Barnes, C.G., Snoko, A.W., Howard, K.A., Frost, C.D., 2003. Petrogenesis of Mesozoic, peraluminous granites in the Lamoille Canyon area, Ruby Mountains, Nevada, USA. *J. Petrol.* 44 (4), 713–732.
- Lee, J., Blackburn, T., Johnston, S., 2017. Timing of mid-crustal ductile extension in the northern Snake Range metamorphic core complex, Nevada: evidence from U/Pb zircon ages. *Geosphere* 13, 439–459.
- Levy, D.A., Zuza, A.V., 2019. Does stress vary in rheologically heterogeneous shear zones? Insight from the mylonites of secret pass, Ruby-East Humboldt metamorphic core complex, Nevada. *GSA Annual Meeting in Phoenix, Arizona, USA*. Geological Society of America Abstracts with Programs 51 <https://doi.org/10.1130/abs/2019AM-339164>.
- Lewis, C.J., Wernicke, B.P., Selverstone, J., Bartley, J.M., 1999. Deep burial of the footwall of the northern Snake Range decollement, Nevada. *Geol. Soc. Am. Bull.* 111, 39–51.
- Li, J., Dong, S., Cawood, P.A., Zhao, G., Johnston, S.T., Zhang, Y., Xin, Y., 2018. An Andean-type retro-arc foreland system beneath northwest South China revealed by SINOPROBE profiling. *Earth Planet. Sci. Lett.* 490, 170–179.
- Long, S.P., 2012. Magnitudes and spatial patterns of erosional exhumation in the Sevier hinterland, eastern Nevada and western Utah, USA: Insights from a Paleogene paleogeologic map. *Geosphere* 8, 881–901.
- Long, S.P., 2015. An upper-crustal fold province in the hinterland of the Sevier orogenic belt, eastern Nevada, USA: a Cordilleran Valley and Ridge in the Basin and Range. *Geosphere* 11, 404–424.

- Long, S.P., 2019. Geometry and magnitude of extension in the Basin and Range Province (39° N), Utah, Nevada, and California, USA: Constraints from a province-scale cross section. *GSA Bull.* 131, 99–119.
- Long, S.P., Kohn, M.J., 2020. Distributed ductile thinning during thrust emplacement: a commonly overlooked exhumation mechanism. *Geology* 48 (4), 368–373.
- Long, S.P., Soignard, E., 2016. Shallow-crustal metamorphism during late cretaceous anatexis in the Sevier hinterland plateau: Peak temperature conditions from the Grant Range, eastern Nevada, USA. *Lithosphere* 8, 150–164.
- Long, S.P., Henry, C.D., Muntean, J.L., Edmondo, G.P., Cassel, E.J., 2014. Early cretaceous construction of a structural culmination, Eureka, Nevada, USA: Implications for out-of-sequence deformation in the Sevier hinterland. *Geosphere* 10, 564–584.
- Long, S.P., Thomson, S.N., Reiners, P.W., Di Fiori, R.V., 2015. Synorogenic extension localized by upper-crustal thickening: an example from the late cretaceous Nevadaplano. *Geology* 43, 351–354.
- Long, S.P., Heizler, M.T., Thomson, S.N., Reiners, P.W., Fryxell, J.E., 2018. Rapid Oligocene to early Miocene extension along the Grant Range detachment system, Nevada, USA: Insights from multipart cooling histories of footwall rocks. *Tectonics* 37 (12), 4752–4779.
- Luisier, C., Baumgartner, L., Schmalholz, S.M., Siron, G., Vennemann, T., 2019. Metamorphic pressure variation in a coherent Alpine nappe challenges lithostatic pressure paradigm. *Nat. Commun.* 10, 1–11.
- Lund Sneek, J.E., Miller, E.L., Grove, M., Hourigan, J.K., Konstantinou, A., 2016. Cenozoic paleogeographic evolution of the Elko Basin and surrounding region, Northeast Nevada. *Geosphere* 12, 464–500.
- MacCready, T., Snoko, A.W., Wright, J.E., Howard, K.A., 1997. Mid-crustal flow during Tertiary extension in the Ruby Mountains core complex, Nevada. *Geol. Soc. Am. Bull.* 109, 1576–1594.
- Marques, F.O., Ranalli, G., Mandal, N., 2018. Tectonic overpressure at shallow depth in the lithosphere: the effects of boundary conditions. *Tectonophysics* 746, 702–715.
- Mazzucchelli, M.L., Burnley, P., Angel, R.J., Morganti, S., Domeneghetti, M.C., Nestola, F., Alvaro, M., 2018. Elastic geothermobarometry: Corrections for the geometry of the host-inclusion system. *Geology* 46, 231–234.
- McGrew, A.J., Sneek, L.W., 1994. ⁴⁰Ar/³⁹Ar thermochronologic constraints on the tectonothermal evolution of the northern East Humboldt Range metamorphic core complex, Nevada. *Tectonophysics* 238, 425–450.
- McGrew, A.J., Snoko, A.W., 2015. Geologic map of the welcome quadrangle and an adjacent part of the Wells quadrangle, Elko County, Nevada. Nevada Bureau of Mines and Geology Map 184.
- McGrew, A.J., Peters, M.T., Wright, J.E., 2000. Thermobarometric constraints on the tectonothermal evolution of the East Humboldt Range metamorphic core complex, Nevada. *Geol. Soc. Am. Bull.* 112, 45–60.
- McGrew, A.J., Metcalf, J.R., Carte, A.J., Jeruc, J.W., 2019. New insights into the time-transgressive extensional exhumation history of the Ruby Mountains-East Humboldt Range metamorphic core complex, Nevada. Geological Society of America, Cordilleran Section, 115th Annual Meeting, Portland, OR, United States, Abstract No. 2–4.
- McQuarrie, N., 2002. The kinematic history of the central Andean fold-thrust belt, Bolivia: Implications for building a high plateau. *Geol. Soc. Am. Bull.* 114, 950–963.
- McQuarrie, N., Wernicke, B.P., 2005. An animated tectonic reconstruction of southwestern North America since 36 Ma. *Geosphere* 1, 147–172.
- Miller, C.F., Bradfish, L.J., 1980. An inner Cordilleran belt of muscovite-bearing plutons. *Geology* 8, 412–416.
- Miller, E.L., Gans, P.B., 1989. Cretaceous crustal structure and metamorphism in the hinterland of the Sevier thrust belt, western US Cordillera. *Geology* 17, 59–62.
- Miller, D.M., Hoisch, T.D., 1995. Jurassic tectonics of northeastern Nevada and northwestern Utah from the perspective of barometric studies. In: Miller, D.M., Busby, C. (Eds.), *Jurassic magmatism and tectonics of the North American Cordillera*: Geological Society of America Special Paper 299, pp. 267–294.
- Miller, E.L., Gans, P.B., Garing, J., 1983. The Snake Range decollement: an exhumed mid-Tertiary ductile-brittle transition. *Tectonics* 2, 239–263.
- Misch, P., Hazzard, J.C., 1962. Stratigraphy and metamorphism of late Precambrian rocks in central northeastern Nevada and adjacent Utah. *AAPG Bull.* 46, 289–343.
- Moulas, E., Podladchikov, Y.Y., Aranovich, L.Y., Kostopoulos, D., 2013. The problem of depth in geology: when pressure does not translate into depth. *Petrology* 21, 527–538.
- Moulas, E., Burg, J.P., Podladchikov, Y., 2014. Stress field associated with elliptical inclusions in a deforming matrix: Mathematical model and implications for tectonic overpressure in the lithosphere. *Tectonophysics* 631, 37–49.
- Moulas, E., Schmalholz, S.M., Podladchikov, Y., Tajčmanová, L., Kostopoulos, D., Baumgartner, L., 2019. Relation between mean stress, thermodynamic, and lithostatic pressure. *J. Metamorph. Geol.* 37, 1–14.
- Mutch, E.J.F., Blundy, J.D., Tattitch, B.C., Cooper, F.J., Brooker, R.A., 2016. An experimental study of amphibole stability in low-pressure granitic magmas and a revised Al-in-hornblende geobarometer. *Contrib. Mineral. Petrol.* 171, 85.
- Nadin, E.S., Saleeby, J., Wong, M., 2016. Thermal evolution of the Sierra Nevada batholith, California, and implications for strain localization. *Geosphere* 12 (2), 377–399.
- Nutt, C.J., Hofstra, A.H., 2003. Alligator Ridge district, east-Central Nevada: Carlin-type gold mineralization at shallow depths. *Econ. Geol.* 98, 1225–1241.
- Odlow, J.S., Bally, A.W., Ave Lallemand, H.G., Leeman, W.P., 1989. Phanerozoic evolution of the North American Cordillera; United States and Canada. In: Bally, A.W., Palmer, A.R. (Eds.), *The Geological Society of America-Vol. A: An Overview. The Geology of North America*, pp. 139–232.
- Oldow, J.S., 1984. Evolution of a late Mesozoic back-arc fold and thrust belt, northwestern Great Basin, U.S.A. *Tectonophysics* 102, 245–274.
- Pattison, D.R., Vogl, J.J., 2005. Contrasting Sequences of Metapelitic Mineral-Assemblages in the aureole of the Tilted Nelson Batholith, British Columbia: Implications for phase equilibria and pressure determination in andalusite-sillimanite-type settings. *Can. Mineral.* 43, 51–88.
- Pattison, D.R., De Capitani, C., Gaidies, F., 2011. Petrological consequences of variations in metamorphic reaction affinity. *J. Metamorph. Geol.* 29 (9), 953–977.
- Perkins, E.H., Brown, T.H., Berman, R.G., 1986. PT-system, TX-system, PX-system: three programs which calculate pressure-temperature-composition phase diagrams. *Comput. Geosci.* 12, 749–755.
- Petrini, K., Podladchikov, Y.Y., 2000. Lithospheric pressure-depth relationship in compressive regions of thickened crust. *J. Metamorph. Geol.* 18, 67–77.
- Pleuger, J., Podladchikov, Y.Y., 2014. A purely structural restoration of the NFP20-East cross section and potential tectonic overpressure in the Adula nappe (central Alps). *Tectonics* 33, 656–685.
- Powell, R., Holland, T.J.B., 1988. An internally consistent dataset with uncertainties and correlations: 3. Applications to geobarometry, worked examples and a computer program. *J. Metamorph. Geol.* 6, 173–204.
- Rhys, D., Valli, F., Burgess, R., Heitt, D., Greisel, G., Hart, K., 2015. Controls of fault and fold geometry on the distribution of gold mineralization on the Carlin trend, in New concepts and discoveries. *Proc. Geol. Soc. Nevada Symp.* 1, 333–389.
- Royce Jr., F., Warner, M.A., Reese, D.L., 1975. Thrust belt structural geometry and related stratigraphic problems, Wyoming-Idaho-northern Utah. *Rocky Mountain Association of Geologists 1975 Symposium*, pp. 41–54.
- Schmalholz, S.M., Podladchikov, Y.Y., 2013. Tectonic overpressure in weak crustal-scale shear zones and implications for the exhumation of high-pressure rocks. *Geophys. Res. Lett.* 40, 1984–1988.
- Schmalholz, S.M., Medvedev, S., Lechmann, S.M., Podladchikov, Y., 2014. Relationship between tectonic overpressure, deviatoric stress, driving force, isostasy and gravitational potential energy. *Geophys. J. Int.* 197, 680–696.
- Schmid, D.W., Podladchikov, Y.Y., 2003. Analytical solutions for deformable elliptical inclusions in general shear. *Geophys. J. Int.* 155, 269–288.
- Schmidt, C., Ziemann, M.A., 2000. In-situ Raman spectroscopy of quartz: a pressure sensor for hydrothermal diamond-anvil cell experiments at elevated temperatures. *Am. Mineral.* 85, 1725–1734.
- Sibson, R.H., 1974. Frictional constraints on thrust, wrench and normal faults. *Nature* 249, 542–544.
- Smith, M.T., Rhys, D., Ross, K., Lee, C., Gray, J.N., 2013. The Long Canyon deposit: Anatomy of a new off-trend sedimentary rock-hosted gold discovery in northeastern Nevada. *Econ. Geol.* 108, 1119–1145.
- Smith, M.E., Cassel, E.J., Jicha, B.R., Singer, B.S., Canada, A.S., 2017. Hinterland drainage closure and lake formation in response to middle Eocene Farallon slab removal, Nevada. *USA: Earth Planet. Sci. Lett.* 479, 156–169.
- Snoko, A.W., 1980. Transition from infrastructure to suprastructure in the northern Ruby Mountains, Nevada. In: Crittenden, M.D., Coney, P.J., Davis, G.H. (Eds.), *Cordilleran Metamorphic Core Complexes*: Geological Society of America Memoir, 153, pp. 287–334.
- Snoko, A.W., 1992. Clover Hill, Nevada: Structural link between the Wood Hills and East Humboldt Range. In: Wilson, J.R. (Ed.), *Field Guide to Geologic Excursions in Utah and Adjacent Areas of Nevada, Idaho, and Wyoming*. Geological Society of America and Utah Geological Survey Miscellaneous Publication 92-3, pp. 107–122.
- Soleymani, H., Kidder, S., Hirth, G., Garapić, G., 2020. The effect of cooling during deformation on recrystallized grain-size piezometry. *Geology* 48, 531–535.
- Spear, F.S., 2017. Garnet growth after overstepping. *Chem. Geol.* 466, 491–499.
- Spear, F.S., Pattison, D.R., 2017. The implications of overstepping for metamorphic assemblage diagrams (MADs). *Chem. Geol.* 457, 38–46.
- Spear, F.S., Selverstone, J., 1983. Quantitative PT paths from zoned minerals: theory and tectonic applications. *Contrib. Mineral. Petrol.* 83, 348–357.
- Stewart, J.H., Poole, F.G., 1974. Lower Paleozoic and uppermost Precambrian Cordilleran miogeoclinal, Great Basin, western United States. In: Dickinson, W.R. (Ed.), *Tectonics and Sedimentation*. The Society of Economic Paleontologists and Mineralogists Special Publication 22, pp. 28–57.
- Tajčmanová, L., Podladchikov, Y., Powell, R., Moulas, E., Vrijmoed, J.C., Connolly, J.A.D., 2014. Grain-scale pressure variations and chemical equilibrium in high-grade metamorphic rocks. *J. Metamorph. Geol.* 32, 195–207.
- Tajčmanová, L., Vrijmoed, J., Moulas, E., 2015. Grain-scale pressure variations in metamorphic rocks: implications for the interpretation of petrographic observations. *Lithos* 216, 338–351.
- Thomas, J.B., Spear, F.S., 2018. Experimental study of quartz inclusions in garnet at pressures up to 3.0 GPa: evaluating validity of the quartz-in-garnet inclusion elastic thermobarometer. *Contrib. Mineral. Petrol.* 173, 42.
- Thorman, C.H., 1970. Metamorphosed and Nonmetamorphosed Paleozoic Rocks in the Wood Hills and Pequoop Mountains, Northeast Nevada: Geological Society of America Bulletin 81, pp. 2417–2448.
- Thorman, C.H., Ketner, K.B., Peterson, Fred, 1990. The Elko orogeny - late Jurassic orogenesis in the Cordilleran miogeoclinal. Geological Society of America, Cordilleran Section Meeting, Tucson, Arizona 22, p. 88.
- Thorman, C.H., Ketner, K.B., Peterson, F., 1992. The Middle to Late Jurassic Elko Orogeny in eastern Nevada and western Utah. Geological Society of America Abstracts with Programs 24.
- Thorman, C.H., Sandberg, C.A., Henry, C.D., Zuza, A.V., Ressel, M.W., 2019. Regional tectonics and conodont CALs indicate normal burial depths, not Mesozoic thickening, in the Pequoop Mountains, NE Nevada. *Geol. Soc. Am. Abstr. Programs* 51.
- Tomkins, H.S., Powell, R., Ellis, D.J., 2007. The pressure dependence of the zirconium-in-rutile thermometer. *J. Metamorph. Geol.* 25, 703–713.
- Van Buer, N.J., Miller, E.L., Dumitru, T.A., 2009. Early Tertiary paleogeologic map of the northern Sierra Nevada batholith and the northwestern Basin and Range. *Geology* 37, 371–374.

- Villien, A., Kligfield, R.M., 1986. Thrusting and synorogenic sedimentation in central Utah. In: Peterson, J.A. (Ed.), *Paleotectonics and Sedimentation in the Rocky Mountain Region*. United States. American Association of Petroleum Geologists Memoir 41, pp. 281–307.
- Vrijmoed, J.C., Podladchikov, Y.Y., Andersen, T.B., Hartz, E.H., 2009. An alternative model for ultra-high pressure in the Svartberget Fe-Ti garnet-peridotite, Western Gneiss Region, Norway. *Eur. J. Mineral.* 21, 1119–1133.
- Wang, C., Gao, R., Yin, A., Wang, H., Zhang, Y., Guo, T., Li, Q., Li, Y., 2011. A mid-crustal strain-transfer model for continental deformation: a new perspective from high-resolution deep seismic-reflection profiling across NE Tibet. *Earth Planet. Sci. Lett.* 306, 279–288.
- Watson, E.B., Wark, D.A., Thomas, J.B., 2006. Crystallization thermometers for zircon and rutile. *Contrib. Mineral. Petrol.* 151, 413.
- Webb, A.A.G., Yin, A., Harrison, T.M., C el erier, J., Burgess, W.P., 2007. The leading edge of the Greater Himalayan Crystalline complex revealed in the NW Indian Himalaya: Implications for the evolution of the Himalayan orogen. *Geology* 35, 955–958.
- Welch, A.H., Bright, D.J., Knochenmus, L.A., 2007. Water resources of the Basin and Range carbonate-rock aquifer system, White Pine County, Nevada, and adjacent areas in Nevada and Utah. US Geological Survey Scientific Investigations Report 5261 pp. 1–96.
- Wells, M.L., 2018. Tectonic inheritance in Cordilleran metamorphic core complex. *Geological Society of America Abstracts with Programs* 50.
- Wells, M.L., Hoisch, T.D., Cruz-Uribe, A.M., Vervoort, J.D., 2012. Geodynamics of synconvergent extension and tectonic mode switching: Constraints from the Sevier-Laramide orogen. *Tectonics* 31, TC1002.
- Wheeler, J., 2014. Dramatic effects of stress on metamorphic reactions. *Geology* 42, 647–650.
- Wheeler, J., 2018. The effects of stress on reactions in the Earth: sometimes rather mean, usually normal, always important. *J. Metamorph. Geol.* 36, 439–461.
- Wills, M.A., 2014. A Metamorphic Pressure-Temperature Time Path from the Wood Hills, Elko County, Eastern Nevada. MS thesis. Northern Arizona University.
- Wright, J.E., Snoke, A.W., 1993. Tertiary magmatism and mylonitization in the Ruby-East Humboldt metamorphic core complex, northeastern Nevada: U-Pb geochronology and Sr, Nd, and Pb isotope geochemistry. *Geol. Soc. Am. Bull.* 105, 935–952.
- Wyld, S.J., Rogers, J.W., Copeland, P., 2003. Metamorphic evolution of the Luning-Fencemaker fold-thrust belt, Nevada: Illite crystallinity, metamorphic petrology, and ⁴⁰Ar/³⁹Ar geochronology. *J. Geol.* 111, 17–38.
- Yamato, P., Brun, J.P., 2017. Metamorphic record of catastrophic pressure drops in subduction zones. *Nat. Geosci.* 10, 46–50.
- Yin, A., 2006. Cenozoic tectonic evolution of the Himalayan orogen as constrained by along-strike variation of structural geometry, exhumation history, and foreland sedimentation. *Earth Sci. Rev.* 76, 1–131.
- Yonkee, W.A., Weil, A.B., 2015. Tectonic evolution of the Sevier and Laramide belts within the north American Cordillera orogenic system. *Earth Sci. Rev.* 150, 531–593.
- Yonkee, W.A., Eleogram, B., Wells, M.L., Stockli, D.F., Kelley, S., Barber, D.E., 2019. Fault Slip and Exhumation history of the Willard Thrust Sheet, Sevier Fold-Thrust Belt, Utah: Relations to Wedge Propagation, Hinterland Uplift, and Foreland Basin Sedimentation. *Tectonics* 38, 2850–2893.
- Zhong, X., Moulas, E., Taj cmanova, L., 2018. Tiny timekeepers witnessing high-rate exhumation processes. *Sci. Rep.* 8 (1), 1–9.
- Zhong, X., Moulas, E., Taj cmanova, L., 2020. Post-entrapment modification of residual inclusion pressure and its implications for Raman elastic thermobarometry. *Solid Earth* 11, 223–240.
- Zuza, A.V., Henry, C.D., Ressel, M.W., Thorman, C.H., Dee, S., Blackmon, J.E., 2018. Preliminary geologic map of the Independence Valley NE quadrangle, Elko County, Nevada. Nevada Bureau of Mines and Geology Open File Report 18-4.
- Zuza, A.V., Dee, S., Henry, C.D., Ressel, M.W., Thorman, C.H., 2019a. Preliminary geologic map of the Independence Valley NW quadrangle, Elko County, Nevada. Nevada Bureau of Mines and Geology Open File Report 19-3.
- Zuza, A.V., Wu, C., Wang, Z., Levy, D.A., Li, B., Xiong, X., Chen, X., 2019b. Underthrusting and duplexing beneath the northern Tibetan Plateau and the evolution of the Himalayan-Tibetan orogen. *Lithosphere* 11, 209–231.
- Zuza, A.V., Cao, W., Hinz, N.H., DesOrmeau, J.W., Odlum, M.L., Stockli, D.F., 2019c. Footwall rotation in a regional detachment fault system: evidence for horizontal-axis rotational flow in the Miocene Searchlight pluton, NV. *Tectonics* 38 (7), 2506–2539.
- Zuza, A.V., Thorman, C.H., Henry, C.D., Levy, D.A., Dee, S., Long, S.P., Sandberg, C., Soignard, E., 2020. Pulsed Mesozoic deformation in the Cordilleran hinterland and evolution of the Nevadaplano: Insights from the Pequop Mountains, NE Nevada. *Lithosphere* <https://doi.org/10.2113/2020/8850336>.